Presynaptic developmental plasticity allows robust sparse wiring of the *Drosophila* mushroom body

Najia A. Elkahlah[1, *], Jackson A. Rogow[2, *], Maria Ahmed[1], and E. Josephine Clowney[1, $]

1. Department of Molecular, Cellular, and Developmental Biology, The University of Michigan, Ann Arbor, MI 48109, USA

2. Laboratory of Neurophysiology and Behavior, The Rockefeller University, New York, NY 10065, USA.

* These authors contributed equally to this work.

$ To whom correspondence should be addressed: jclowney@umich.edu

Abstract: In order to represent complex stimuli, principle neurons of associative learning regions receive combinatorial sensory inputs. Density of combinatorial innervation is theorized to determine the number of distinct stimuli that can be represented and distinguished from one another, with sparse innervation thought to optimize the complexity of representations in networks of limited size. How the convergence of combinatorial inputs to principle neurons of associative brain regions is established during development is unknown. Here, we explore the developmental patterning of sparse olfactory inputs to Kenyon cells of the *Drosophila melanogaster* mushroom body. By manipulating the ratio between pre- and post-synaptic cells, we find that postsynaptic Kenyon cells set convergence ratio: Kenyon cells produce fixed distributions of dendritic claws while presynaptic processes are plastic. Moreover, we show that sparse odor responses are preserved in mushroom bodies with reduced cellular repertoires, suggesting that developmental specification of convergence ratio allows functional robustness.

Introduction: The environmental stimuli animals encounter on a day-to-day basis are extraordinarily numerous. Olfactory systems have evolved to cope with this diversity by maximizing the chemicals that can be detected, through the amplification of chemosensory receptor gene families, and through combinatorial coding, which expands representation capacity from the number of receptors in the genome to the number of combinations among them. The arthropod mushroom body is a cerebellum-like associative learning structure with a well-understood role in representing sensory stimuli and associating sensory and contextual cues (Farris, 2011; Hige, 2018; Kennedy, 2015). While mushroom bodies of different insect species process information from a variety of sensory modalities, 90% of Kenyon cell inputs in *Drosophila melanogaster* are olfactory (Zheng et al., 2018). The mushroom body of each hemisphere has ~2000 Kenyon cells (KCs), which are two synapses from the sensory periphery. Each olfactory receptor neuron in the antennae of adult flies expresses one or two of 75 olfactory receptor genes encoded in the genome. The axons of neurons expressing the same receptor converge on one of 50 glomeruli

in the antennal lobe. ~150 uniglomerular projection neurons (PNs) have dendrites in one of the 50 glomeruli and carry signals about distinct receptor channels to two regions of the protocerebrum, the lateral horn and the mushroom body calyx (Figure 1A). PN inputs to the lateral horn are thought to underlie innate behaviors, while inputs to the mushroom body allow flexible learned association of odor stimuli with behavioral context (Chin et al., 2018; de Belle and Heisenberg, 1994; Fişek and Wilson, 2014; Jefferis et al., 2007; Ruta et al., 2010).

In the mushroom body calyx, the presynaptic sites of individual olfactory PNs cluster into multisynaptic boutons, with PNs of different types (innervating different glomeruli) producing consistent, characteristic bouton numbers (Caron et al., 2013; Zheng et al., 2018). Each PN makes 1-20 boutons, and each bouton is wrapped by claws of ~10 KCs, such that each PN sends output to between 10 and 200 of the 2000 KCs (Leiss et al., 2009). KCs in turn have 3-10 (average of five) claws, which innervate boutons of various PNs (Caron et al., 2013; Gruntman and Turner, 2013; Zheng et al., 2018). Each KC therefore receives innervation from only a minority of the 50 incoming sensory channels, and different individual KCs receive different and relatively unstructured combinations of inputs (Caron et al., 2013; Eichler et al., 2017; Honegger et al., 2011; Murthy et al., 2008; Zheng et al., 2018). The sets of inputs to individual cells vary across hemispheres and likely across individuals (Caron et al., 2013; Eichler et al., 2017; Honegger et al., 2011; Murthy et al., 2008). Associative learning mechanisms operate at KC output synapses, in the mushroom body axonal lobes, to re-weight KC outputs depending on experience and shift animal behavior (Cohn et al., 2015; Handler et al., 2019; Hige et al., 2015; Owald and Waddell, 2015).

The mushroom body is a simplified and experimentally tractable example of an expansion layer, in which a set of sensory inputs is mapped combinatorially onto a much larger set of postsynaptic cells, increasing the dimensionality of sensory representations. Like the diversification of

68 antibodies by V(D)J recombination, the diversification of sensory input combinations across KCs
69 is thought to allow them to represent arbitrary odors, regardless of evolutionary experience.
70 Neurons of many other expansion layers receive similarly few, or sparse, sensory inputs. These
71 include the cerebellum proper, the electric organ of mormyrid fish, the dorsal cochlear nucleus,
72 and the hippocampus (Bell et al., 2008; Keene and Waddell, 2007; Mugnaini et al., 1980). Cere-
73 bellar granule cells have an average of four large, claw-shaped dendrites that are innervated by
74 clustered mossy fiber presynaptic sites in mossy fiber rosettes. The similar convergence ratios
75 in the cerebellum and mushroom body (4 or 5 sensory inputs, respectively, per expansion layer
76 cell) are thought to maximize dimensionality of sensory representations by optimizing the
77 tradeoff between stimulus representation, which is maximized when expansion layer neurons
78 receive large combinations of inputs, and stimulus separation, which is maximized when expan-
79 sion layer neurons receive few inputs (Albus, 1971; Cayco-Gajic et al., 2017; Litwin-Kumar et
80 al., 2017; Marr, 1969). The number of sensory inputs received by expansion layer neurons is
81 thus a crucial parameter in sensory coding. How the density of inputs to expansion layer neu-
82 rons is developmentally programmed is not understood in any system.
83
84 Innervation complexity more generally has been studied in the peripheral nervous system and in
85 the developing mammalian cortex. In peripheral sensory neurons, most prominently those of the
86 *Drosophila* larval body wall, cell-autonomous mechanisms profoundly influence dendritic com-
87 plexity (Corty et al., 2016; Jan and Jan, 2010; Ziegler et al., 2017). However, sensory neurons
88 do not need to coordinate their innervation with presynaptic partners. In the vertebrate periph-
89 eral nervous system, including the rabbit ciliary ganglion and vertebrate neuromuscular junction,
90 postsynaptic neurons or muscles are thought to dictate wiring complexity (Gibbins et al., 2003;
91 Hume and Purves, 1983, 1981; Purves and Hume, 1981; Turney and Lichtman, 2012). In con-
92 trast, in the developing cortex, extracellular signals including BDNF play a strong role in influ-
93 encing dendritic complexity, suggesting that presynaptic cells and glia also influence

connectivity density (Kohara et al., 2003; McAllister et al., 1997, 1995; Purves, 1986). Therefore, while mechanisms acting in both pre- and post-synaptic cells *can* influence innervation complexity, there is a need to directly compare how pre- and post-synaptic cells influence one another.

We sought to ask how convergence ratio is set in the mushroom body calyx. By bidirectionally varying the populations of pre- and post-synaptic cells, we were able to make many different mushroom body aberrations. Across these conditions, we found a consistent pattern of compensations: the number of claws per KC remained largely constant, while the number of presynaptic boutons per olfactory PN varied bidirectionally and in response to changes of both the PN and KC populations. We therefore conclude that in this circuit, connectivity density is set by aspects of KC specification and is accomplished by flexible innervation of the calyx by PNs.

Results: In order to ask whether presynaptic olfactory PNs or postsynaptic KCs (or both) dictate sparse wiring density in the mushroom body calyx, we used a variety of methods to manipulate the ratio between pre- and post-synaptic cells during embryonic or larval stages, well before adult connections form in the pupa. Through a combination of genetic and pharmacological interventions, we were able to vary both cell populations up and down. In these four conditions, we then examined gross calyx anatomy in adult animals and, when possible, the processes of individual PNs and KCs. These experiments allowed us to ask which population of neurons would adjust its production of processes in response to the perturbation. As we will describe, in all four cases, PNs adjusted their repertoire of presynaptic sites while KC claw number remained similar to that of unmanipulated animals.

Projection neurons reduce bouton number when Kenyon cell number is reduced

119 First, we sought to reduce the KC population, to ask whether remaining cells would increase
120 their claw number to fully innervate incoming PN boutons, or whether PNs would scale down
121 their boutons to the KC repertoire. To do this, we took advantage of existing pharmacological
122 techniques for KC neuroblast ablation (de Belle and Heisenberg, 1994; Sweeney et al., 2012).
123 In the fly, four KC neuroblasts in each hemisphere produce ~500 KCs each (Ito et al., 1997).
124 While most neuroblasts pause their divisions for the first 8 hours after larval hatching (ALH), the
125 KC neuroblasts continue to divide; if larvae are fed the mitotic poison hydroxyurea during this
126 time, KC neuroblasts can be specifically ablated (de Belle and Heisenberg, 1994). In these ani-
127 mals, lacking all KCs that receive olfactory inputs, olfactory learning is abrogated while innate
128 olfactory behaviors are spared (de Belle and Heisenberg, 1994). The uniglomerular, excitatory
129 olfactory PNs that innervate the MB calyx are produced by two neuroblasts, called lNB/BAlc and
130 adNB/BAmv3 . Besides the KC neuroblasts, lNB/BAlc is the only other neuroblast in the fly cen-
131 tral nervous system dividing from 0-8h ALH and is thus also susceptible to HU ablation (Das et
132 al., 2013; Ito and Hotta, 1992; Lovick et al., 2016; Lovick and Hartenstein, 2015; Stocker et al.,
133 1997; Sweeney et al., 2012).
134
135 While ablation of all eight KC neuroblasts (4/hemisphere) was used to demonstrate the role of
136 KCs in olfactory learning (de Belle and Heisenberg, 1994), we sought to perform more subtle
137 manipulations of the mushroom body cell populations. We generated animals in which PNs and
138 KCs were fluorescently labeled to facilitate scoring, and reduced the concentration and duration
139 of HU application, producing mushroom bodies with a variety of Kenyon cell complements, likely
140 due to sporadic loss of different neuroblast complements in each hemisphere (Figure 1B).
141 Together, these neuroblast losses could potentially produce 1-2 PN neuroblasts and mushroom
142 bodies derived from 0-4 KC neuroblasts. Using our reporters, we scored the presence or ab-
143 sence of PNs ventrolateral to the antennal lobe, derived from lNB/BAlc, and counted the number
144 of KCs (Figure 1C). In practice, some of the neuroblast states did not occur and some were

145 overrepresented (Figure 2-figure supplement 1). Hemispheres from the same brain did not gen-
146 erally show the same neuroblast state as one another, but were often similar in severity of neu-
147 roblast losses (Figure 2-figure supplement 1).
148
149 KCs of different types are produced in a characteristic sequence in development: γ KCs are
150 born in the embryo and early larva, α'β' KCs are born in late larvae, and αβ KCs are born in pu-
151 pae. We identified samples in which all 4 KC neuroblasts had been ablated by looking for sam-
152 ples lacking mushroom body vertical lobes, which are composed of axons of α'β' and αβ KCs
153 and thus do not form if all KC neuroblasts are killed by HU just after hatching. We confirmed
154 previous findings that in animals with all four KC neuroblasts ablated, the PNs fail to target the
155 calyx and project only to the lateral horn (Stocker et al., 1997). In these animals, ~100 KCs re-
156 mained (Figure 1B). These represent the KC population that is born prior to larval hatching, and
157 which is thus unaffected by KC neuroblast ablation after hatching. Recently, these earliest-born
158 cells, called γd KCs, have been shown to receive visual and not olfactory input in adult flies
159 (Vogt et al., 2016; Yagi et al., 2016). These observations suggest that γd KCs are molecularly
160 distinct from later-born cells during pupal calyx wiring, such that even when all the olfactory KCs
161 are absent, olfactory PNs cannot innervate visual KCs. Remarkably, these embryonic-born γd
162 KCs receive olfactory inputs in the early larva and are sufficient for olfactory learning at that time
163 (Eichler et al., 2017; Pauls et al., 2010); they must therefore switch their partner preferences
164 across developmental stages.
165
166 We then examined calyx anatomy in animals with intermediate populations of KCs, likely de-
167 rived from 1-3 remaining neuroblasts. We found a progressive decrease in the size of the mush-
168 room body calyx in these animals as measured by the maximum cross-sectional area of the ca-
169 lyx (Figure 1B, C) or by calyx volume (Figure 1-figure supplement 1, Figure 1-video 1). To ask if

170 this corresponded to a decline in bouton number, we counted the number of PN boutons in each
171 hemisphere (Figure 1E, Figure 1-figure supplement 2). This revealed a linear relationship be-
172 tween KC number and PN bouton number, suggesting that PNs reduce their population of bou-
173 tons to match the KC population. The lateral horn appeared normal in these animals and its size
174 did not correlate with KC number, suggesting that PN projections to these two brain areas de-
175 velop independent of one another (Figure 1B, D). The presence or absence of ventrolateral PNs
176 did not obviously predict bouton number, suggesting individual PNs may be able to tailor their
177 bouton production both to the number of KCs and to adjust to the number of other PNs. How-
178 ever, we were not able to obtain enough samples to draw firm conclusions about whether PN
179 cell number affected PN bouton number in calyces derived from matched KC neuroblast com-
180 plements. To test this, we developed alternative methods to ablate PNs (Figure 5, 6).
181

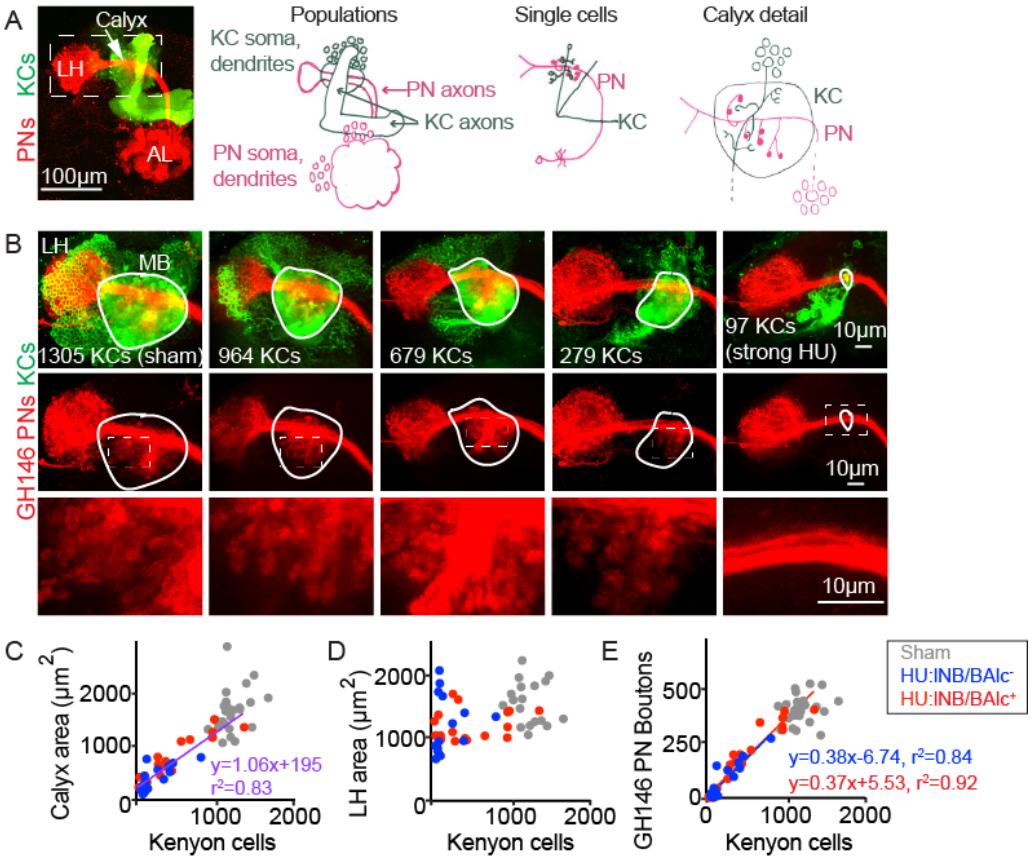

182

Figure 1: Reduction of Kenyon cells leads to reduced projection neuron innervation of the mushroom body calyx. (A) Images (left) and models (right) of olfactory PNs and KCs in the adult fly brain. PNs (red) receive input from olfactory sensory neurons in the antennal lobe (AL) and project to the mushroom body calyx and the lateral horn (LH). In the calyx, PNs synapse with KCs (green) in microglomeruli. Dashed box at left indicates region shown in B. (B) Maximum intensity projections of confocal stacks of the brains of adult flies subjected to HU treatment or sham treatment just after larval hatching. PNs labeled red using GH146-Gal4, KCs green using MB247-LexA. White outlines indicate the extent of the MB calyx in each sample; dashed boxes are regions shown magnified below. (C, D) Relationship between number of KCs and calyx (C) or lateral horn (D) maximum cross-sectional area in HU treated (blue, red dots) and sham treated (grey dots) MBs. Treated samples are separated by presence (red) or absence (blue) of INB/BAlc progeny. Here and throughout, each dot is one hemisphere. Purple trend line in (C) combines all HU-treated samples. (E) Relationship between KC number and GH146+ bouton number in brains of HU- and sham-treated animals.

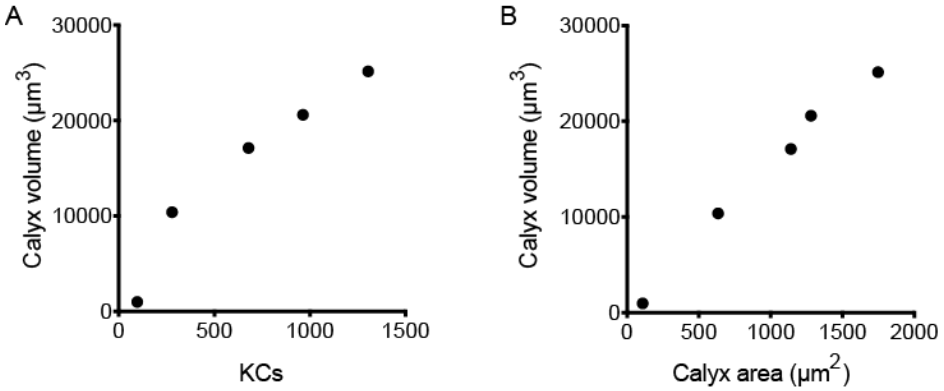

Figure 1-figure supplement 1 (A) Correlation between KC number and calyx volume for the samples shown in Figure 1B and Figure 1-video 1. (B) Correlation between calyx maximum cross-sectional area and calyx volume for samples shown in Figure 1B and Figure 1-video 1.

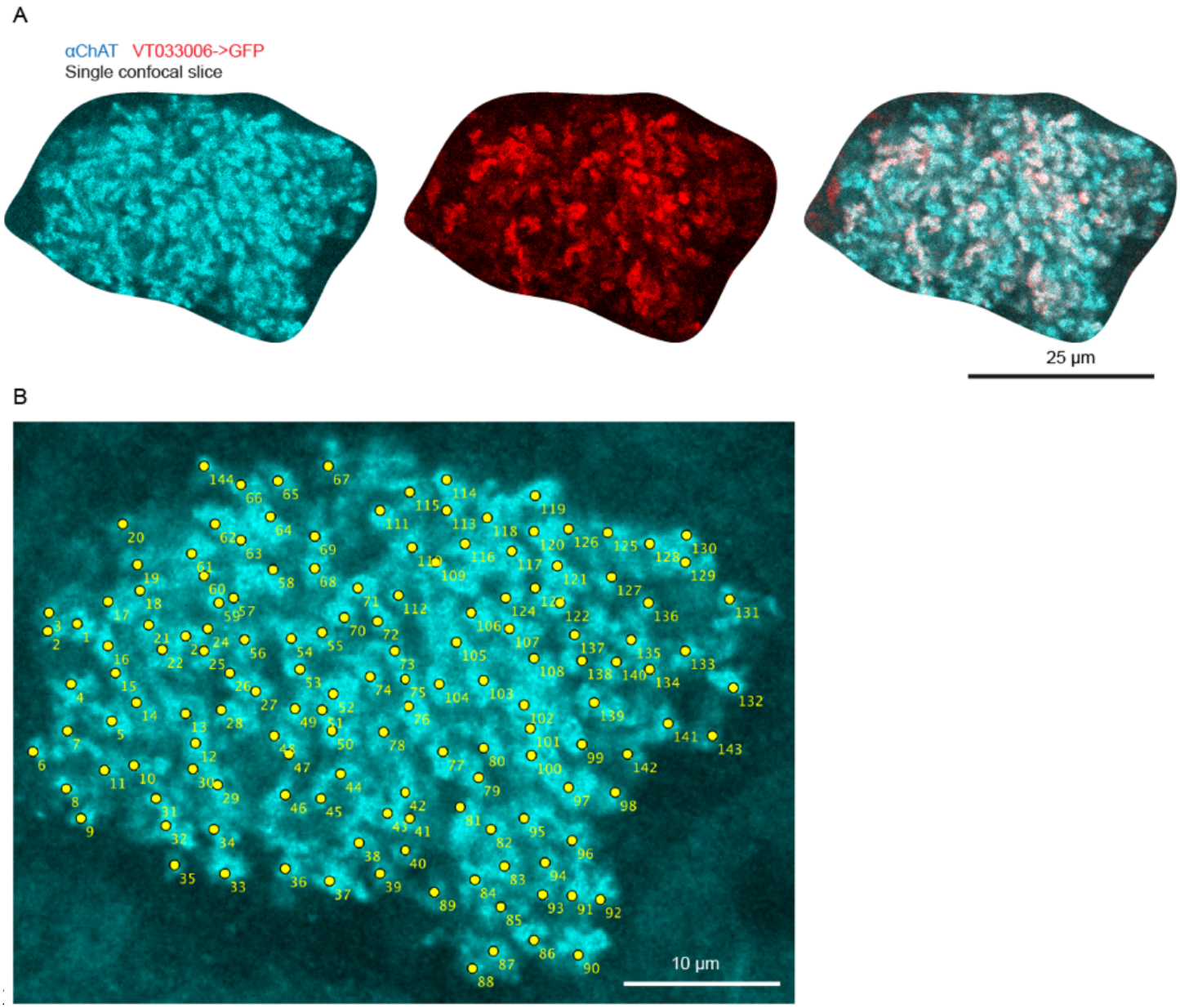

Figure 1-figure supplement 2. High-resolution images of calyx boutons (A) and example of bouton counting for a single confocal plane (B); each yellow dot was scored as a bouton.

To score KC clones directly, we developed a strategy to label only the latest-born, "αβ core" KCs. The somata and principle neurites of these late-born cells remain clustered in the adult, allowing us to count KC clones by counting groups of labeled soma or axon tracts as they leave the calyx (Figure 2A, B). Again, we found that calyx size tracked KC clone number, and that the presence or absence of the PN progeny of lNB/BAlc did not predict calyx size (Figure 2C). KC

211 loss could reduce PN bouton number because PNs die or fail to be born when lacking KC con-
212 tacts or trophic support. We thus counted the number of anterodorsal PNs (derived from
213 adNB/BAmv3) and ventrolateral PNs (derived from lNB/BAlc) in this cohort. The number of an-
214 terodorsal PNs was not reduced in animals with some or all KC neuroblasts ablated, and the
215 number of ventrolateral PNs was binary rather than graded, suggesting that vlPN number is de-
216 termined by whether lNB/BAlc succumbed to HU, rather than by the KC complement (Figure
217 2D, E). These results suggest that PN neurogenesis and survival do not require KC signals.
218 Like γd KCs, a few PNs derived from lNB/BAlc remained in adults; these likely represent PNs
219 born embryonically from lNB/BAlc.
220
221 Reduction in the number of PN boutons in the calyx could occur because individual PNs quanti-
222 tatively reduce their bouton production. To ask whether individual PNs alter their production of
223 presynaptic boutons as the KC repertoire changes, we identified two methods to label single
224 PNs. We focused on anterodorsal PNs, as these are not susceptible to ablation of lNB/BAlc.
225 First, we used 71D09 Gal4 to label the anterodorsal VM6 PN (Ward et al., 2015) and then sub-
226 jected labeled animals to HU ablation. Because we found a linear relationship between KC num-
227 ber and calyx area (Figure 1C, 2C), we used calyx area as a proxy for KC number. While VM6
228 usually produces ~10 boutons, we found only ~5 boutons in animals with reduced calyx size,
229 and 0-1 bouton in animals with severe calyx reductions, likely lacking all olfactory KCs (Figure
230 2F-H). These results suggest that individual PNs do reduce their bouton production as the KC
231 complement is reduced, and that this reduction is graded rather than binary (i.e. in animals with
232 some but not all KC neuroblasts ablated, bouton number is in between 0 and the wild type num-
233 ber). To characterize additional PNs, we expressed photoactivatable GFP under control of
234 R42D01-Gal4, which labels ~10 anterodorsal PNs innervating the VM3 and VM4 glomeruli. We
235 photoconverted individual somata using two photon microscopy (Figure 2-figure supplement 2).
236 Though bouton counts were somewhat more variable than for VM6 as this strategy labels

237 different types of PNs with different characteristic bouton numbers, we again found a correlation
238 between KC loss and bouton reduction (Figure 2-figure supplement 2).
239
240 The graded reductions in bouton number we observed for different PN types would preserve the
241 relative representation of these odor channels in the calyx. While the genetic constraints of
242 these experiments prevented us from scoring the status of lNB/BAlc, we also note that the
243 range of bouton numbers we observed are consistent with adjustments to compensate for the
244 presence or absence of ventrolateral PNs. For example, most VM6 neurons innervating a calyx
245 derived from 1 KC neuroblast produced between 3 and 7 boutons, as compared to the median
246 of 10 in unperturbed animals. If KCs are reduced by ¾ without loss of lNB/BAlc, perfect com-
247 pensation by PNs would reduce boutons from 10 to 2.5. If lNB/BAlc was also lost, perfect com-
248 pensation would reduce boutons from 10 to 5. These predicted values are similar to the bouton
249 range we observed experimentally.
250
251 Finally, we sought to ask if KC claw number changes as KC number changes. We used GFP
252 photoactivation to label individual KCs in animals subjected to HU ablation. The different KC
253 classes have different median claw numbers: γ KCs have ~7 claws, αβ cells have ~5 claws, and
254 α'β' KCs have ~3 claws (Caron et al., 2013); we therefore used two different strategies to label
255 individual KCs in animals subjected to HU ablation, both of which allow us to assign KC type.
256 First, we expressed PA-GFP broadly in Kenyon cells using MB247-Gal4, and assigned KC type
257 by imaging the axonal lobe innervation of photoactivated cells (Figure 2-figure supplement 3).
258 Second, we expressed PA-GFP only in αβ or γ KCs using 58F02-Gal4 (Figure 2I) and 89B01-
259 Gal4, respectively. Combining data from these two methods, we found no change in claw num-
260 ber on individual αβ KCs (Figure 2J-K) or γ KCs (Figure 2-figure supplement 3) as the KC popu-
261 lation was reduced. From these experiments, we conclude that PNs reduce their bouton

262 production on a cell-by-cell basis as the KC population shrinks, while KC claw number is unaf-

263 fected by the size of the KC population (model, Figure 2L).

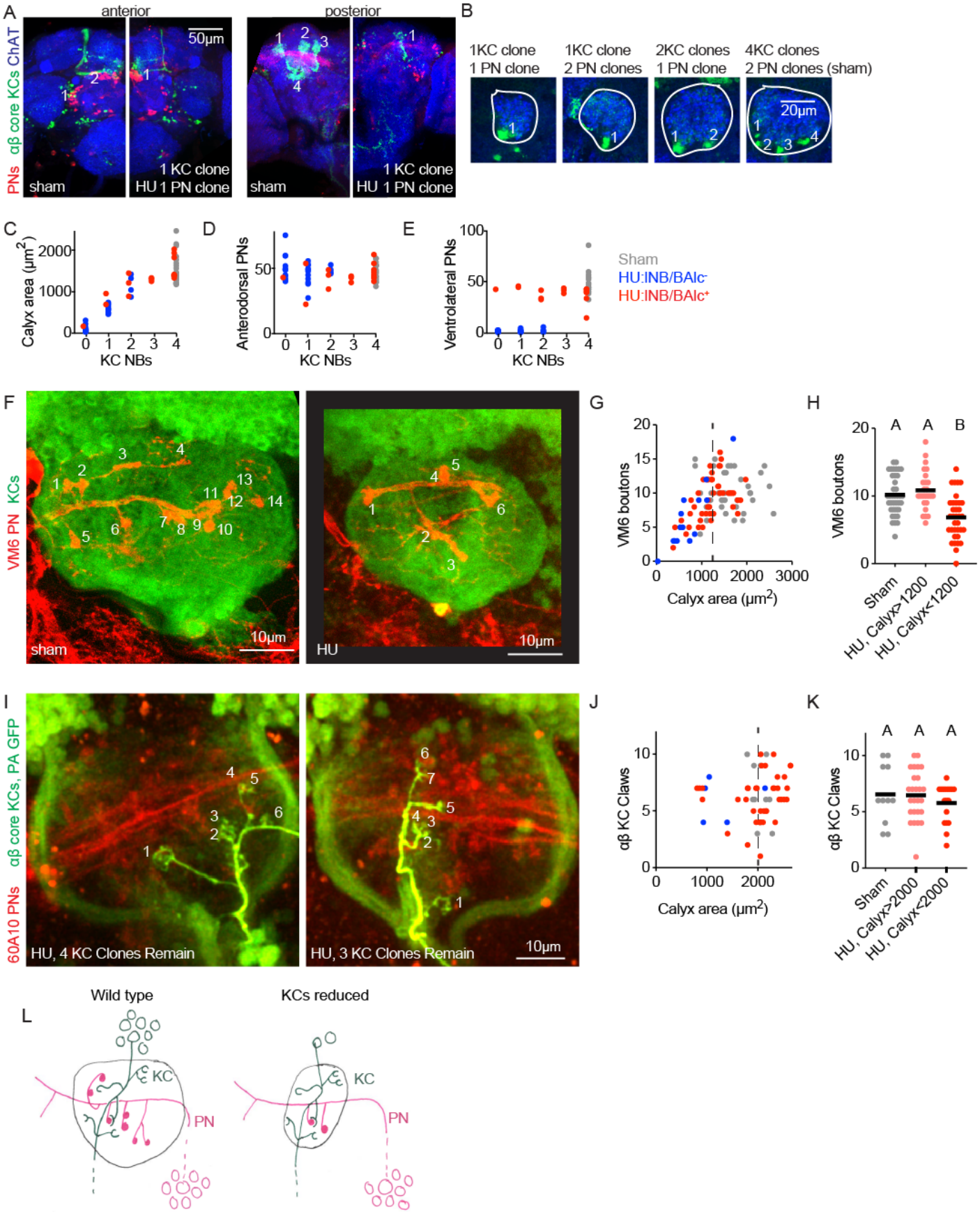
A
anterior
posterior
PNs αβ core KCs ChAT
50μm
1 KC clone
HU 1 PN clone
sham
B
1KC clone
1 PN clone
1KC clone
2 PN clones
2KC clones
1 PN clone
4KC clones
2 PN clones (sham)
20μm
C
Calyx area (μm²)
KC NBs
D
Anterodorsal PNs
KC NBs
E
Ventrolateral PNs
KC NBs
Sham
HU:INB/BAlc⁻
HU:INB/BAlc⁺
F
VM6 PN KCs
sham
HU
10μm
G
VM6 boutons
Calyx area (μm²)
H
VM6 boutons
Sham
HU, Calyx>1200
HU, Calyx<1200
I
αβ core KCs, PA GFP
60A10 PNs
HU, 4 KC Clones Remain
HU, 3 KC Clones Remain
10μm
J
αβ KC Claws
Calyx area (μm²)
K
αβ KC Claws
Sham
HU, Calyx>2000
HU, Calyx<2000
L
Wild type
KCs reduced
KC
PN

264

Figure 2: Individual projection neurons scale their bouton repertoire to the Kenyon cell population. (A) Maximum intensity projections of confocal stacks of the anterior (left) and posterior (right) of HU and sham-treated animals. GH146 labels PNs (red). 58F02 labels late-born αβ "core" KCs (green). Cholinergic neurons labeled with ChAT immunostaining (blue). Numbers indicate PN and KC clones. Anterior and posterior images are of the same brains. (B) Confocal slices of the mushroom body calyx in sham-treated (right) and various HU treated (left) hemispheres. ChAT signal highlights bouton structures, while 58F02 signal allows scoring of the number of KC clones. Numbered neurite bundles innervate the pedunculus when traced through the stack, while green signals not numbered derive from non-KC cell types labeled by 58F02. (C-E) Relationship between KC clone number and maximum calyx cross-sectional area (C), and number of anterodorsal (D) and ventrolateral (E) PNs. (F-H) Example images (F) and quantification (G, H) of MB calyx boutons on the VM6 PN, labeled by 71D09 (red). KCs labeled by MB247 (green). Numbers in (F) indicate counted boutons, and these two calyces are displayed at the same scale. Dashed vertical lines in (G) indicate cutoff between HU-treated calyces similar to controls and those affected by the manipulation. Significance, one-way ANOVA with correction for multiple comparisons. Here and throughout, letters above scatterplots indicate statistically distinguishable versus undistinguishable groups by ANOVA. Black horizontal bars represent medians. (I-K) Example images (I) and quantification (J, K) of GFP photoactivation of individual KCs in HU treated or sham brains. PNs labeled by 60A10 and αβ "core" KCs by 58F02. Examples in (I) show two hemispheres of the same HU treated brain. Note that calyx area is larger in brains imaged *ex vivo* by two photon (as in I-K) versus fixed, stained, and imaged by confocal (as in F-H). Quantification in (J, K) includes αβ KCs labeled as shown in (I) and those labeled as shown in Figure 2-figure supplement 3; quantification of γ KCs labeled by both methods is shown in Figure 2-figure supplement 3. INB/BAlc status was scored by examining PN somata near the antennal lobe, as in (A). (L) Model of the effect of KC loss on calyx development. Remaining KCs exhibit wild-type numbers of claws, while PNs reduce their bouton repertoire, reducing the size of the calyx.

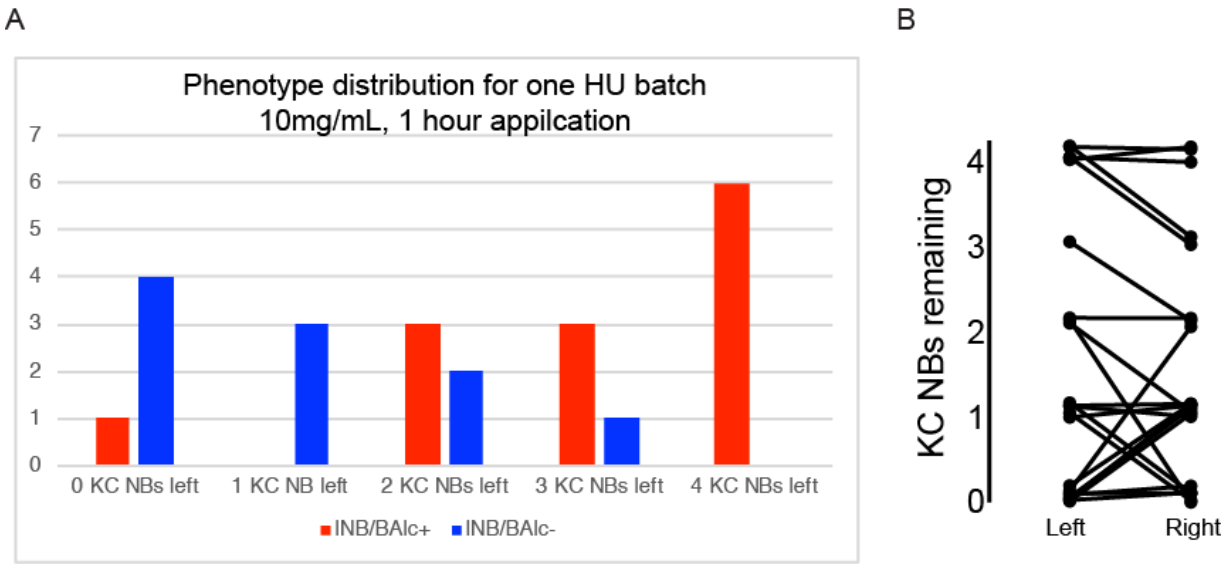

Figure 2-figure supplement 1 (A) Distribution of HU effects for one batch of treated animals. Genotype as in Figure 2A. (B) Relationship of KC neuroblast state across hemispheres. Jitter was added to make each sample apparent.

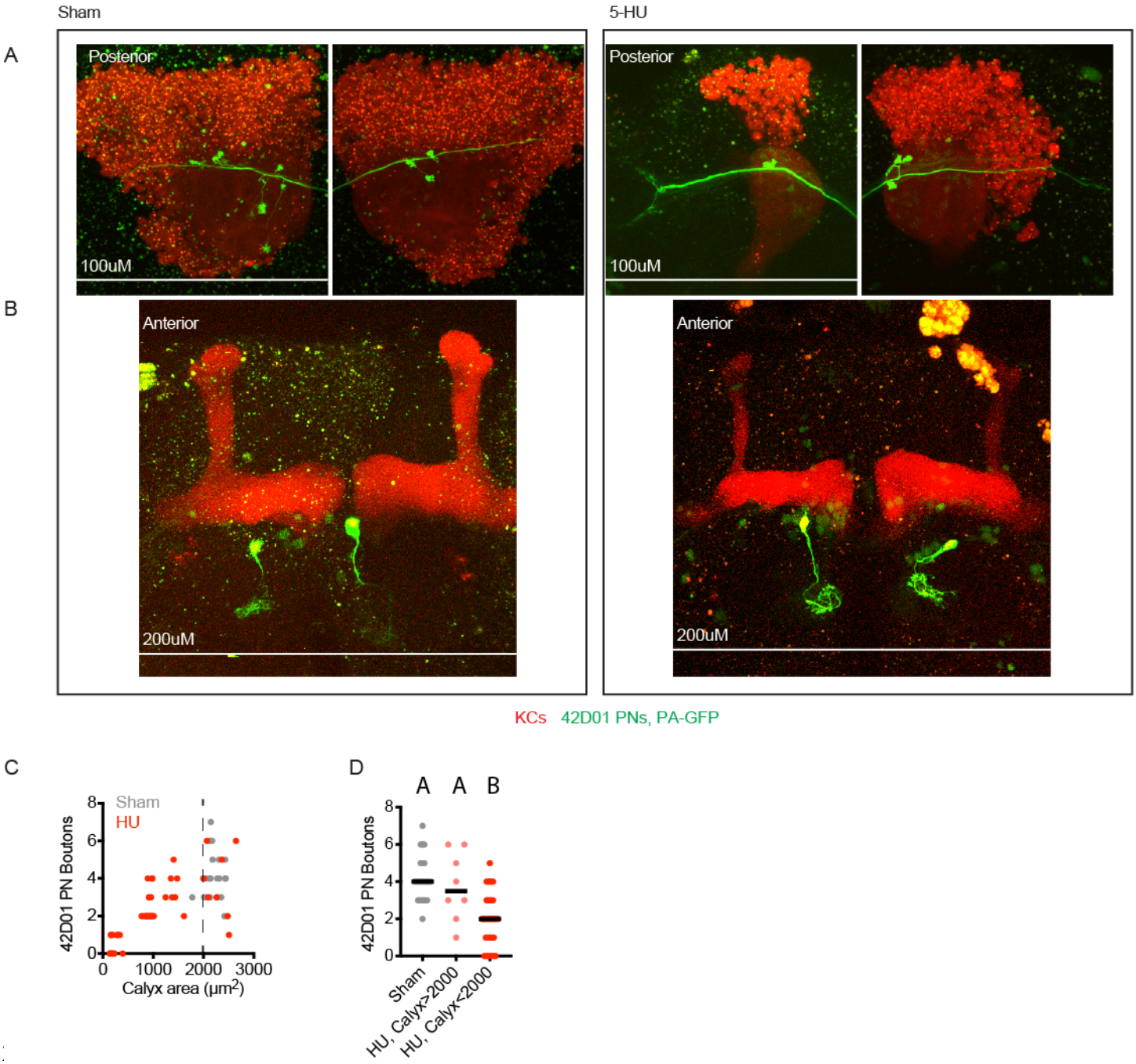

Figure 2-figure supplement 2. Example maximum intensity projections of two photon images (A, B) and quantification (C, D) of PNs labeled by 42D01-Gal4 and highlighted by GFP photoactivation. Each panel shows posterior (A) and anterior (B) images of the same brain, where anterior images show single photoactivated PN somata and glomerular innervation in the antennal lobe, as well as mushroom body lobes, and posterior images show boutons of the same PN in the mushroom body calyx. Speckles are autofluorescence, large yellow blobs are photodamage incurred during imaging. Black horizontal bars in (C,D) represent medians.

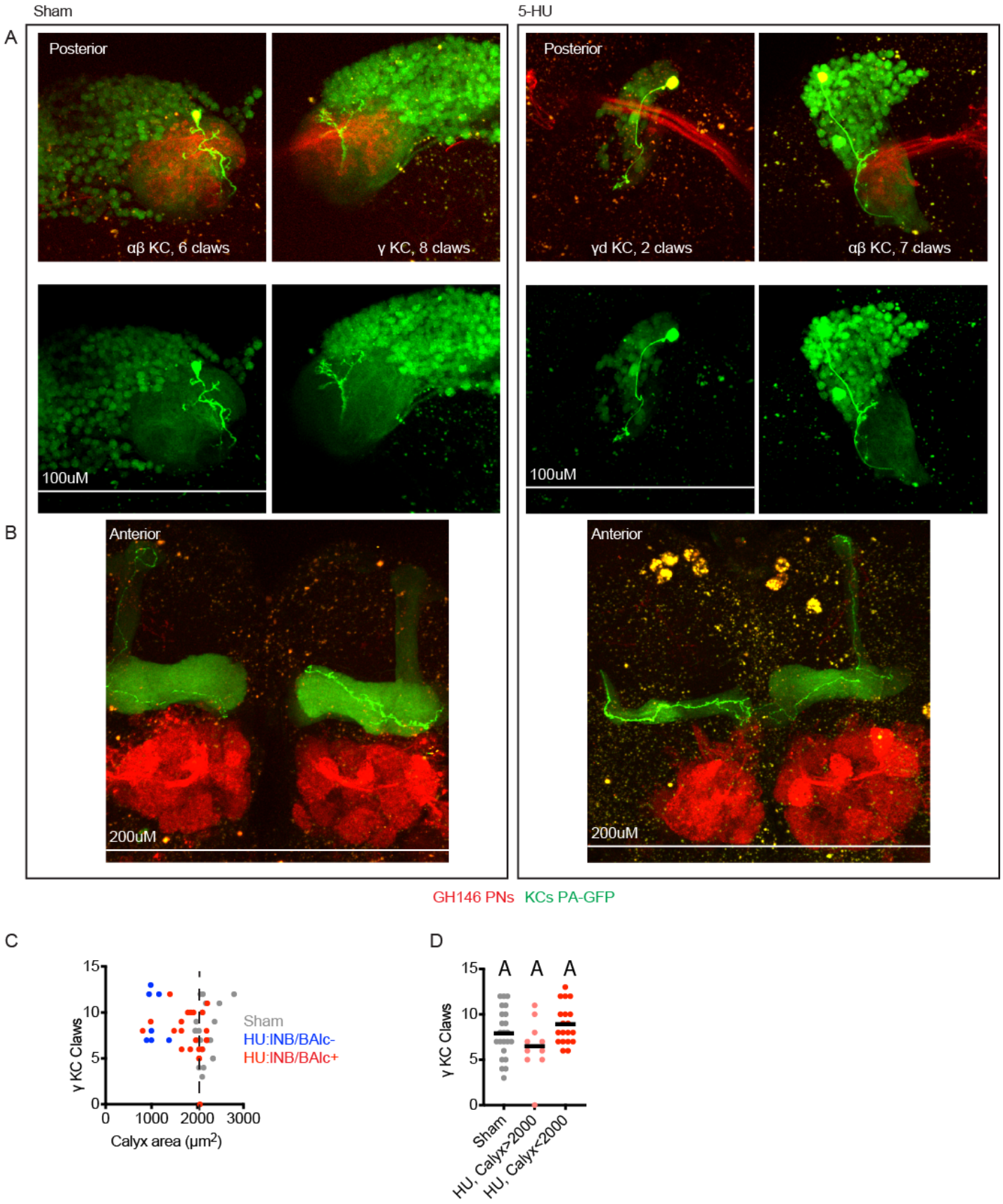
Sham
5-HU
A
Posterior
αβ KC, 6 claws
γ KC, 8 claws
Posterior
γd KC, 2 claws
αβ KC, 7 claws
100uM
100uM
B
Anterior
200uM
Anterior
200uM
GH146 PNs KCs PA-GFP
C
γ KC Claws
Calyx area (μm2)
Sham
HU:INB/BAlc-
HU:INB/BAlc+
D
γ KC Claws
A A A
Sham
HU, Calyx>2000
HU, Calyx<2000

306 **Figure 2-figure supplement 3.** (A, B) Example maximum intensity projections of two photon
307 images of KCs labeled by MB247-LexA and highlighted by GFP photoactivation. Each panel
308 shows posterior (A) and anterior (B) images of a single brain, where anterior images show KC
309 innervation of the mushroom body axonal lobes, as well as the antennal lobe, and posterior im-
310 ages show claws of the same KC in the mushroom body calyx, as well as PN boutons. Axonal
311 lobe innervation allowed us to assign KC type, as noted. Speckles are autofluorescence, large
312 yellow blobs are photodamage incurred during imaging. The left hemisphere of the HU-treated
313 sample is fully ablated and lacks lNB/BAlc progeny, while the right hemisphere is partially ab-
314 lated and retains lNB/BAlc. (C, D) Quantification of claws of γ KCs labeled using the strategy
315 shown here or through expression of PA-GFP only in γ KCs, driven by 89B01-Gal4. lNB/BAlc
316 status scored by examining GH146-Gal4 or 60A10-LexA, as shown in Figure 2A. Black horizon-
317 tal bars represent medians.
318

319 **Olfactory projection neurons increase bouton repertoire as Kenyon cell number in-**
320 **creases**

321 In order to assess whether PNs can vary their presynaptic bouton number bidirectionally, we
322 next created a method to specifically amplify the KC population. Recent work has suggested
323 that ectopic or supernumerary populations of neurons can integrate into a variety of fruit fly neu-
324 ral circuits (Meng et al., 2019; Pop et al., 2019; Prieto-Godino et al., 2019; Seroka and Doe,
325 2019; Shaw et al., 2018), and previous studies identified a mutant, called *mushroom body de-*
326 *fect* (*mud*) in which the mushroom body and other brain areas are dramatically expanded
327 (Guan et al., 2000; Prokop and Technau, 1994). Mud/NuMA is a spindle orientation protein that
328 ensures neuroblasts divide asymmetrically to produce one neuroblast and one differentiating
329 neuron or neural progenitor (Siller et al., 2006). In *mud* mutants, neuroblasts occasionally divide
330 symmetrically to produce two neuroblasts, amplifying the progeny of that neuroblast. To restrict
331 amplification to KCs, we drove UAS-*mud*-RNAi (BL 35044) using OK107-Gal4, which is ex-
332 pressed in KC neuroblasts as well as in KCs (Liu et al., 2015). Importantly, in RNAseq data from
333 45h APF and adult animals, we observe no expression of *mud* in PNs, KCs, or other brain cells,
334 suggesting *mud* is not expressed in differentiating neurons (data not shown).
335

336 As OK107 labels mature KCs as well as KC neuroblasts, we included UAS-CD8GFP in these
337 animals to count KCs. This produced potent amplification of KCs that was variable across

338 animals, sometimes more than doubling KC number (Figure 3A, B). We measured calyx size,
339 which expanded dramatically, and used GH146-driven fluorescence to count PN bouton num-
340 ber, which doubled in mushroom bodies with the largest KC expansions (Figure 3C, Figure 3-
341 video 1). These results suggest that just as PNs scale down their boutons if the KC population is
342 reduced, PNs scale up their boutons when the KC population is expanded.
343
344 To test whether PNs increased boutons on a cell-by-cell basis in these animals, we labeled VM6
345 using 71D09-LexA, and PNs innervating DA1, Va1d, and DC3 using MZ19-QF. First, we ob-
346 served no change in VM6 or MZ19+ cell numbers in brains with KC expansions (Figure 3E, H),
347 suggesting that PN numbers do not increase as KC number increases. We observed no change
348 in VM6 bouton numbers, perhaps because the VM6 PN already has a relatively large number of
349 boutons (Figure 3H). In contrast, MZ19 cells increased their number of presynaptic boutons as
350 the KC population expanded, from an average of 3.5 boutons per cells in the control genotype
351 to an average of 4.75 boutons per cell in the KC-expansion genotype. In brains with enlarged
352 calyces, indicative of KC population expansion, MZ19+ boutons doubled (Figure 3D, F, G).
353
354 To rule out reductions in the number of claws per KC as the KC population expands, we ex-
355 pressed photoactivatable GFP under the control of OK107 in animals with UAS-*mud*-RNAi or
356 control and subjected individual or small groups of KCs to photoactivation. We scored the num-
357 ber of claws per labeled KC in each calyx. As above, calyx size predicted KC number in these
358 animals, so we used calyx size as a proxy for KC number. Rather than a decrease in claw num-
359 ber per KC in animals with expanded KC complements, we found a slight increase in claw num-
360 ber, from a median of 5 to a median of 6 claws. As different types of KCs produce different char-
361 acteristic numbers of claws, this could represent a change in claw production, a change in the
362 distribution of KC types in these animals, or bias in which KC types we labeled in expanded vs
363 control brains. While we were unable to identify LexA lines to specifically label $\alpha\beta$ or γ KCs in

364 OK107->mudRNAi brains, we found a LexA line, R41C07, that labeled α'β' KCs, and targeted
365 these specifically for photoactivation (Figure 3-figure supplement 1). In these KCs of matched
366 type, we found no change in KC claw number per cell, though we cannot rule out subtle differ-
367 ences. Together, these experiments suggest that in animals with an amplified KC complement,
368 PNs dramatically increase their bouton production to match the KC population, while KCs may
369 moderately increase, and do not reduce, their individual claw production.

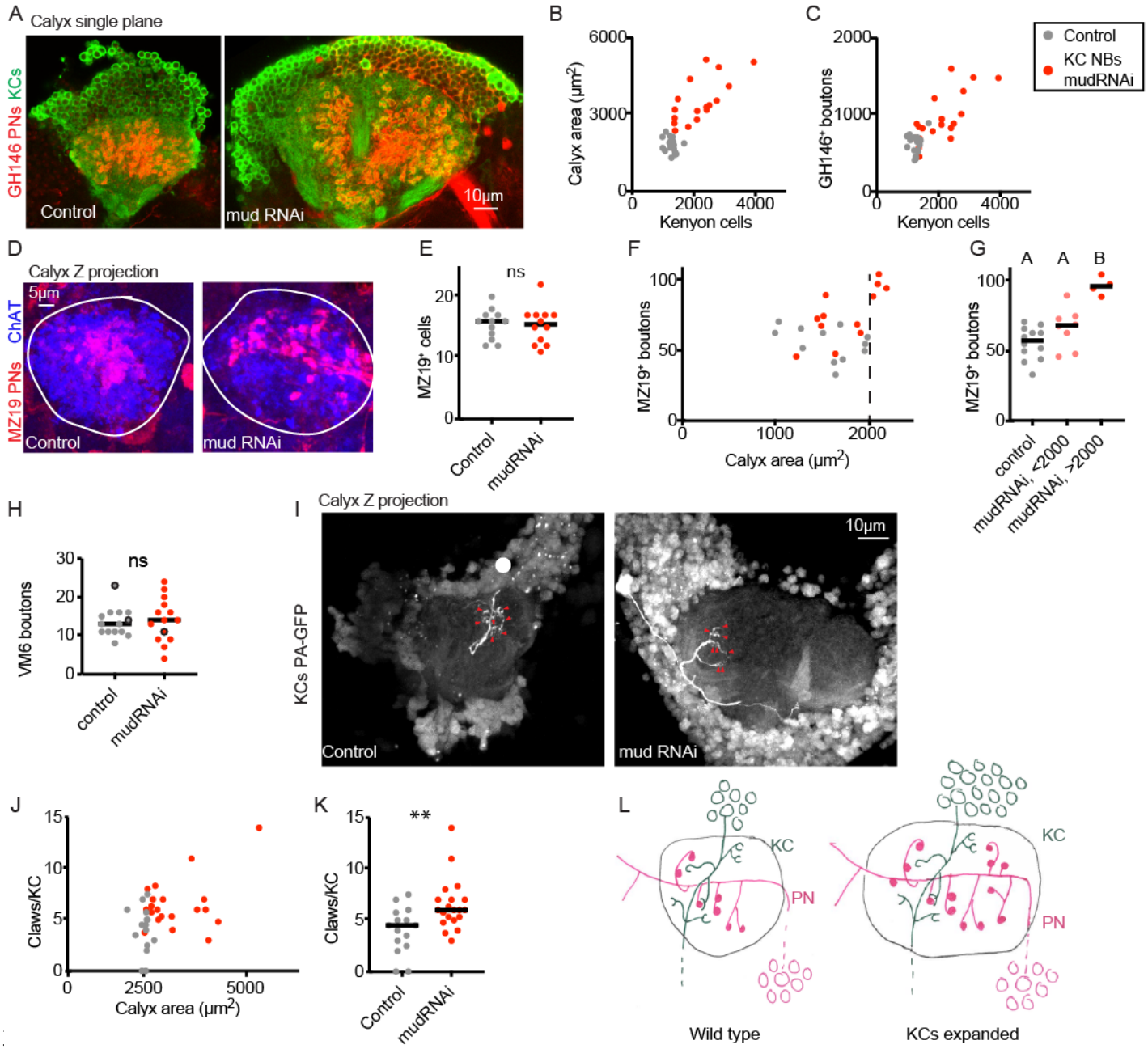

371 **Figure 3: Increase in Kenyon cell number leads to increased projection neuron bouton**
372 **complement.** (A) Confocal slice of control calyx and calyx subjected to KC expansion by ex-
373 pression of *mud*-RNAi in KC neuroblasts via OK107-Gal4. GH146 labels PNs (red) and OK107
374 labels KCs (green). (B, C) Relationship between number of KCs and maximum calyx cross-sec-
375 tional area (B) and PN bouton number (C) in control (grey) and KC neuroblast->mud-RNAi hem-
376 ispheres (red). (D) Maximum intensity projection of confocal stack of calyx bouton production
377 by ~16 MZ19+ PNs (red) in control and KC neuroblast->mud-RNAi. ChAT immunostaining
378 (blue) highlights calyx extent. (E) Quantification of MZ19 cells in the two genotypes. Signifi-
379 cance: unpaired t-test. Throughout this figure, black horizontal bars represent medians. (F, G)
380 Relationship between maximum calyx cross-sectional area and MZ19 bouton production. Verti-
381 cal dashed line indicates calyces larger than 2000 μm^2,observed only in the experimental geno-
382 type. Significance: one-way ANOVA. (H) Boutons of the VM6 PN, labeled by 71D09-LexA, in
383 control (grey) or brains subjected to KC expansion via OK107->mudRNAi (red). Every hemi-
384 sphere contained one VM6 neuron in both genotypes except the three circled datapoints, which
385 had two VM6 PNs. Significance: unpaired t-test. (I) Maximum intensity projection of two-photon
386 stack of single KCs highlighted by GFP photoactivation (C3PA driven by OK107) in control or
387 OK107 ->mudRNAi calyces. Position of out-of-plane somata in control image indicated by white
388 circle. Red arrowheads indicate scored claws. (J, K) Quantification of claws of KCs labeled as in
389 (I). Y axis is average number of claws per KC as multiple KCs were photoactivated in some
390 samples. Significance: unpaired t-test; here and throughout, *: p<0.05, **: p<0.01, ***: p<0.001,
391 ****: p<0.0001. (L) Model of the effect of KC expansion on calyx development. KCs retain nor-
392 mal claw numbers while PNs increase their bouton numbers, increasing calyx size.
393
394

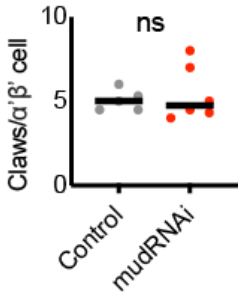

395
396 **Figure 3-figure supplement 1** KC claw number in PA-GFP-labeled α'β' KCs in control or KC-
397 expansion genotype. Significance: unpaired t-test. Black horizonal bars represent medians.
398
399
400 **Individual projection neurons decrease bouton number as the projection neuron popula-**
401 **tion expands**
402 We have shown that olfactory PNs bidirectionally vary their presynaptic boutons to suit popula-
403 tions of KCs derived from 0-8 KC neuroblasts. To ask whether PNs can also vary their bouton
404 production in response to changes in their own numbers, or in response to changes in the ratio
405 between PNs and KCs that do not affect KC clone number, we identified methods to vary the
406 PN population. We found that just as we could expand the KC population by knocking down

407 *mud* in KC neuroblasts, we could expand the PN population by knocking down *mud* in PN neu-
408 roblasts. This strategy produced GH146-labeled PN complements of up to 600 cells, as com-
409 pared to ~120 GH146-labeled PNs we counted in controls. While the PN neuroblast Gal4 we
410 used, 44F03, can label both lNB/BAlc and adNB/BAmv3 progeny (Awasaki et al., 2014), we
411 found that ventrolateral PNs were much more susceptible to expansion than anterodorsal PNs.
412
413 Supernumerary PNs innervated the antennal lobe, causing a massive expansion of antennal
414 lobe area (Figure 4A, C). The normal glomerular map in the AL appeared distorted, but glomer-
415 ular divisions were still present. These PNs also projected to the calyx, observed by thickening
416 of the PN axon tract crossing the calyx (red, Figure 4D), and increased the density of PN inner-
417 vation of the lateral horn (Figure 4D), though not lateral horn area (Figure 4-figure supplement
418 1). However, there was no change in calyx area or total bouton number in these animals com-
419 pared to wild type (Figure 4E-H). At a population level, the average number of boutons per PN
420 was half that in controls (Figure 4I).
421
422 To ask how small groups of PNs adjusted to PN expansion, we again used MZ19-QF, which la-
423 bels 15-20 PNs in controls (Figure 4J, K). We counted MZ19+ cells and boutons in control ver-
424 sus animals of the expansion genotype (Figure 4K). As the expansion was highly variable and
425 we rarely observed more than 25 MZ19+ cells in controls, we divided the expanded genotype
426 into hemispheres with <25 PNs or >=25 PNs. There was a modest but insignificant increase in
427 MZ19+ boutons in the >=25 PNs groups (Figure 4L), attributable to a strong and significant re-
428 duction of average number of boutons per PN (Figure 4M). Thus PNs scale down their individ-
429 ual bouton repertoire to compensate for increases in the size of the PN population. Like MZ19
430 PNs, the VM6 PN also maintained a stable number of total boutons as the PN population ex-
431 panded (Figure 4-figure supplement 1). This was possible because the VM6 cell(s) had similar
432 numbers of total boutons as the VM6 population expanded.

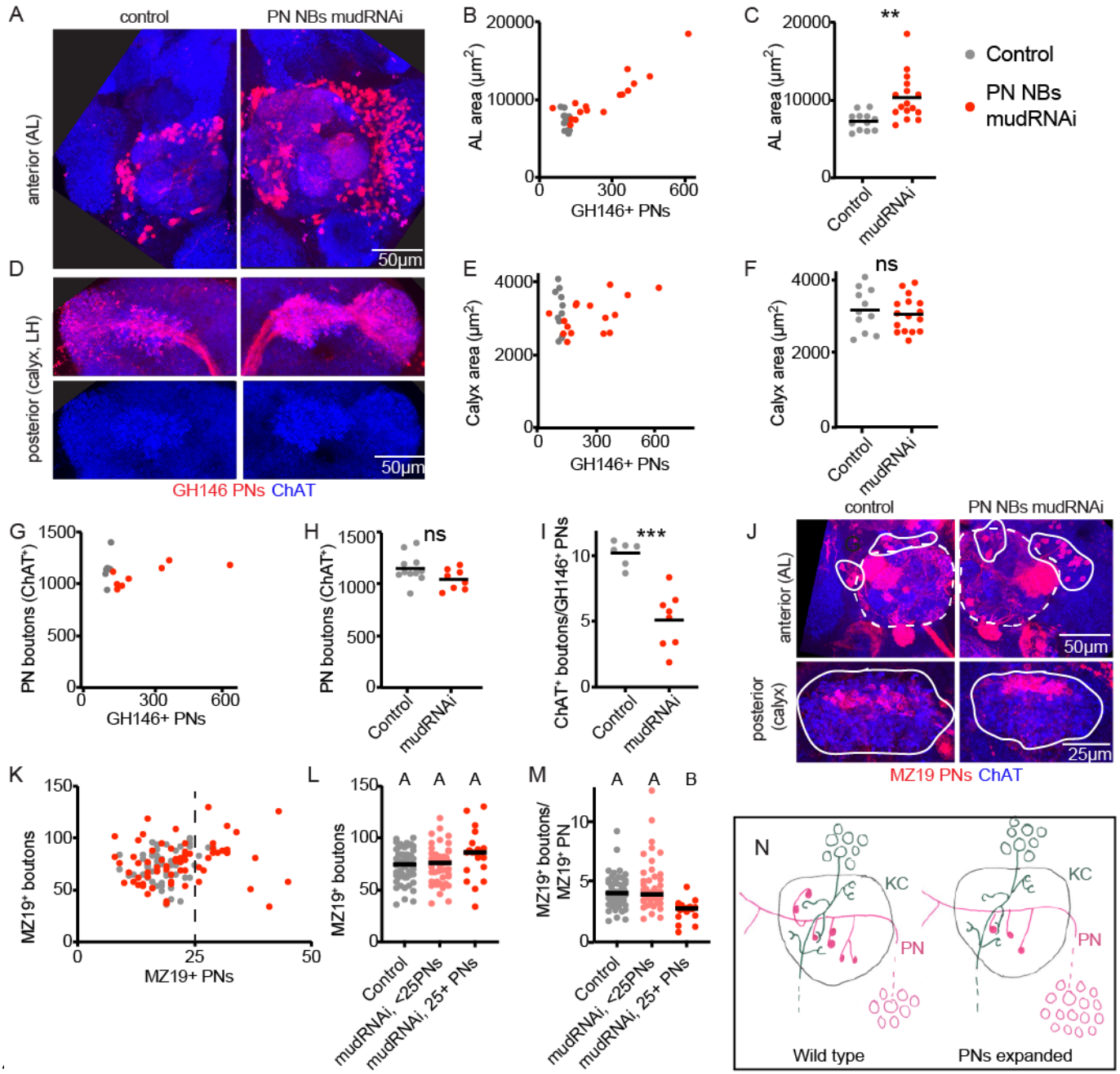

Figure 4: Individual projection neurons scale boutons down as projection neuron population increases. (A) Maximum intensity projection of confocal stack of anterior of the brain of control or animal subjected to PN expansion by expression of *mud*-RNAi in PN neuroblasts via 44F03-Gal4. GH146 labels PNs (red) and ChAT staining highlights cholinergic neurons. (B, C) Relationship between PN number (measured by counting GH146+ cells, about 60% of the total PNs) and antennal lobe maximum cross-sectional area in control (grey) or PN neuroblast->mudRNAi hemispheres (red). Significance: unpaired t-test. Throughout this figure, black horizontal bars represent medians. (D) Maximum intensity projection of confocal stacks of the posteriors of the same brains shown in A. Excess PNs can be seen to project to the calyx, due to thickening of the axonal tract passing on top of the calyx (red), and produce increased innervation density in the lateral horn. (E-I) Relationship between PN number and maximum cross-

445 sectional area of the calyx (E, F), PN bouton number (G, H), and ratio of ChAT+-boutons to
446 GH146+ PNs (I) in control and PN neuroblast->mudRNAi brains. Significance: unpaired t-test.
447 (J) Maximum-intensity projections of confocal stacks of antennal lobes (top) and calyces (bot-
448 tom) of control and PN neuroblast->mudRNAi brains. MZ19+ PNs labeled red. Dashed outlines
449 on anterior show antennal lobe extent; solid outline on anterior, groups of PN somata; solid out-
450 lines on posterior, calyx extent. (K-M) Quantification of MZ19+ boutons in control and PN neuro-
451 blast->mudRNAi brains. Dashed vertical line indicates 25 MZ19+ PNs, as controls seldom ex-
452 ceed this number. Significance: one-way ANOVA. (N) Model of the effect of increasing PN num-
453 bers on calyx development. As PNs increase, PNs reduce bouton production so that the overall
454 number of boutons, and calyx size, stays similar to wild type.
455

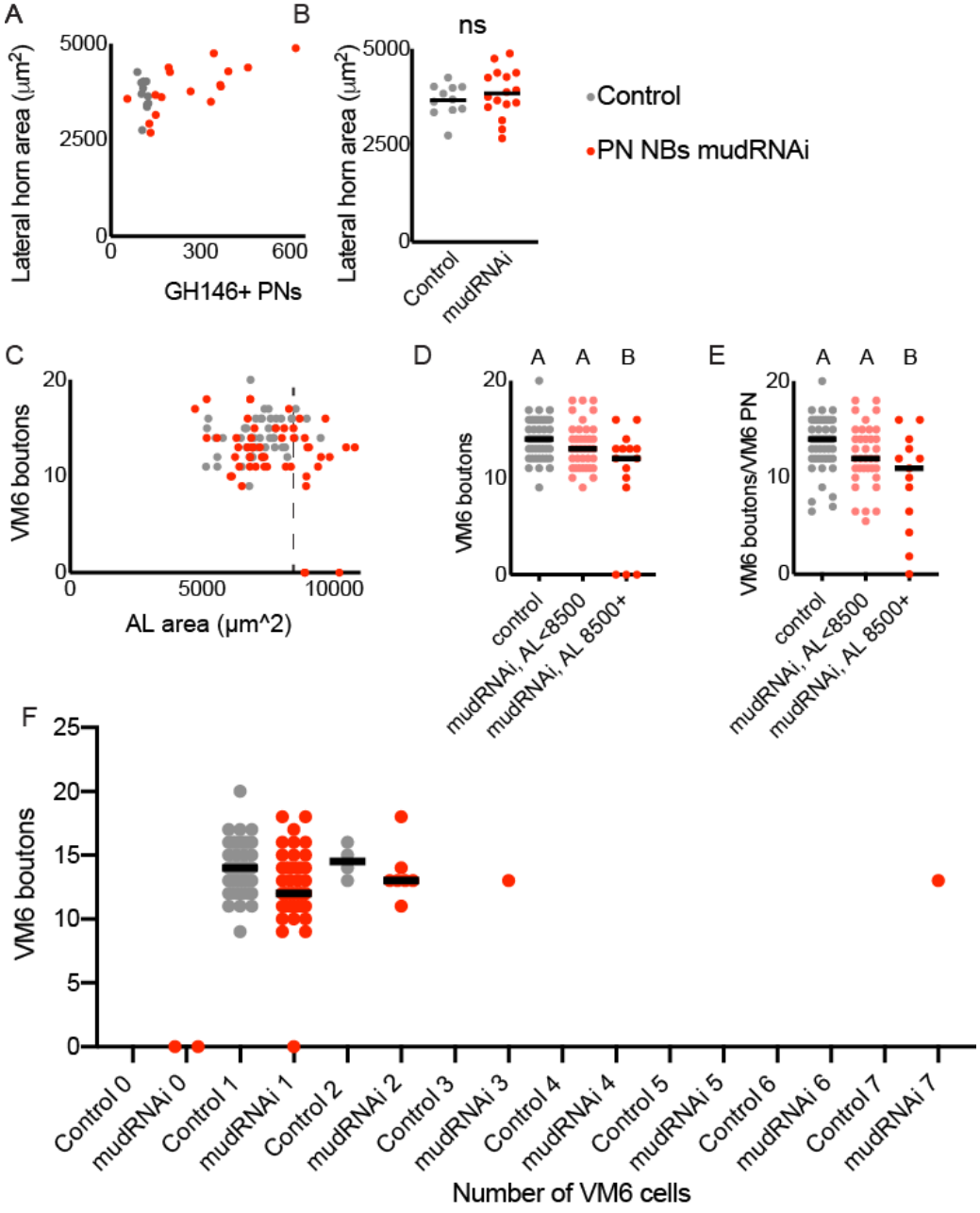

456

457 **Figure 4-figure supplement 1** (A, B) Relationship between lateral horn maximum cross-sec-
458 tional area and PN number in control (grey) and PN neuroblast->mudRNAi (red) brains. Signifi-
459 cance: unpaired t-test. Throughout this figure, black horizontal bars represent medians. (C-E)
460 Relationship between antennal lobe maximum cross-sectional area (proxy for PN number) and
461 production of calyx boutons by the VM6 PN, labeled by 71D09. Dashed line indicates 8500 μm^2,
462 as antennal lobes larger than this were observed rarely in the control genotype. Significance:
463 one-way ANOVA. In two experimental hemispheres, we observed no VM6 PN. In one hemi-
464 sphere, we observed one VM6 PN with no boutons in the calyx. (F) VM6 boutons in calyces of
465 brains containing different numbers of VM6 PNs. We observed more than one VM6 PN in 4/50
466 control and 9/50 PN neuroblast->mudRNAi hemispheres.
467

468 **Projection neuron bouton expansion partially compensates for severe reductions in the**
469 **projection neuron population**

470 In order to reduce the PN repertoire independent of KC number, we identified two Gal4 lines,
471 VT033006 and VT033008, that label large PN complements in the adult (Figure 5A). We drove
472 diphtheria toxin A (Berdnik et al., 2006) and fluorescent reporters under control of these lines in
473 animals where additional PNs were labeled by GH146-LexA (Figure 5B, G). In each case, DTA
474 eliminated all Gal4+ cells as well as additional GH146+ PNs, suggesting that these lines drive
475 DTA expression in broader PN populations at earlier stages of development. Driving DTA under
476 control of VT033008 reduced the total PNs labeled by VT033008 and/or GH146 by nearly half
477 (Figure 5C), while VT033006->DTA reduced PNs labeled by VT03006 and/or GH146 by >90%
478 (Figure 5H). PN labeling by VT033006 and VT033008, and cell loss when used to drive DTA,
479 were already evident in third instar larvae, suggesting PNs are lost well before pupal calyx wir-
480 ing (Figure 5-figure supplement 1). While PN dendrites have been shown to occupy glomerular
481 territories in pupal stages before OSNs innervate the antennal lobe (Jefferis et al., 2004), we
482 found that antennal lobes lacking the vast majority of uniglomerular PNs retained glomerular di-
483 visions. This suggests that PNs may not be required for the formation of glomerular divisions in
484 the adult antennal lobe.
485

486 We measured maximum calyx cross-sectional area and bouton number across these conditions
487 and found that in each case, the effect on the calyx was measurable but much less severe than

488 the reduction in PN number. For VT033008->DTA, loss of nearly half the PNs yielded no
489 change in calyx area and a 20% reduction in overall bouton number (Figure 5D-F). Remarkably,
490 while we estimate that only ~10 PNs remain in VT033006->DTA animals (~7% the normal com-
491 plement, Figure 5H), the number of boutons in the calyx was reduced by only half (Figure 5H,
492 L). This suggests that individual PNs could have expanded their bouton production by as much
493 as 6-fold. While remaining PNs sometimes appeared to make exuberant collections of boutons
494 (e.g. Figure 6D), distortion of the antennal lobes in these animals prevented us from assigning
495 identities to these spared PNs and comparing bouton numbers to matched individual PNs in
496 controls.
497
498 This severe loss of inputs could lead to KC death. We therefore labeled and counted KCs in
499 VT033006->DTA animals with severe PN loss. While we cannot rule out a small reduction in KC
500 complement, at least 80% of KCs survived in these brains. We also subjected control and
501 VT033006->DTA brains to flow cytometry and found that PN ablation brains had at least 85% as
502 many KCs as did control brains (Figure 5-figure supplement 2).

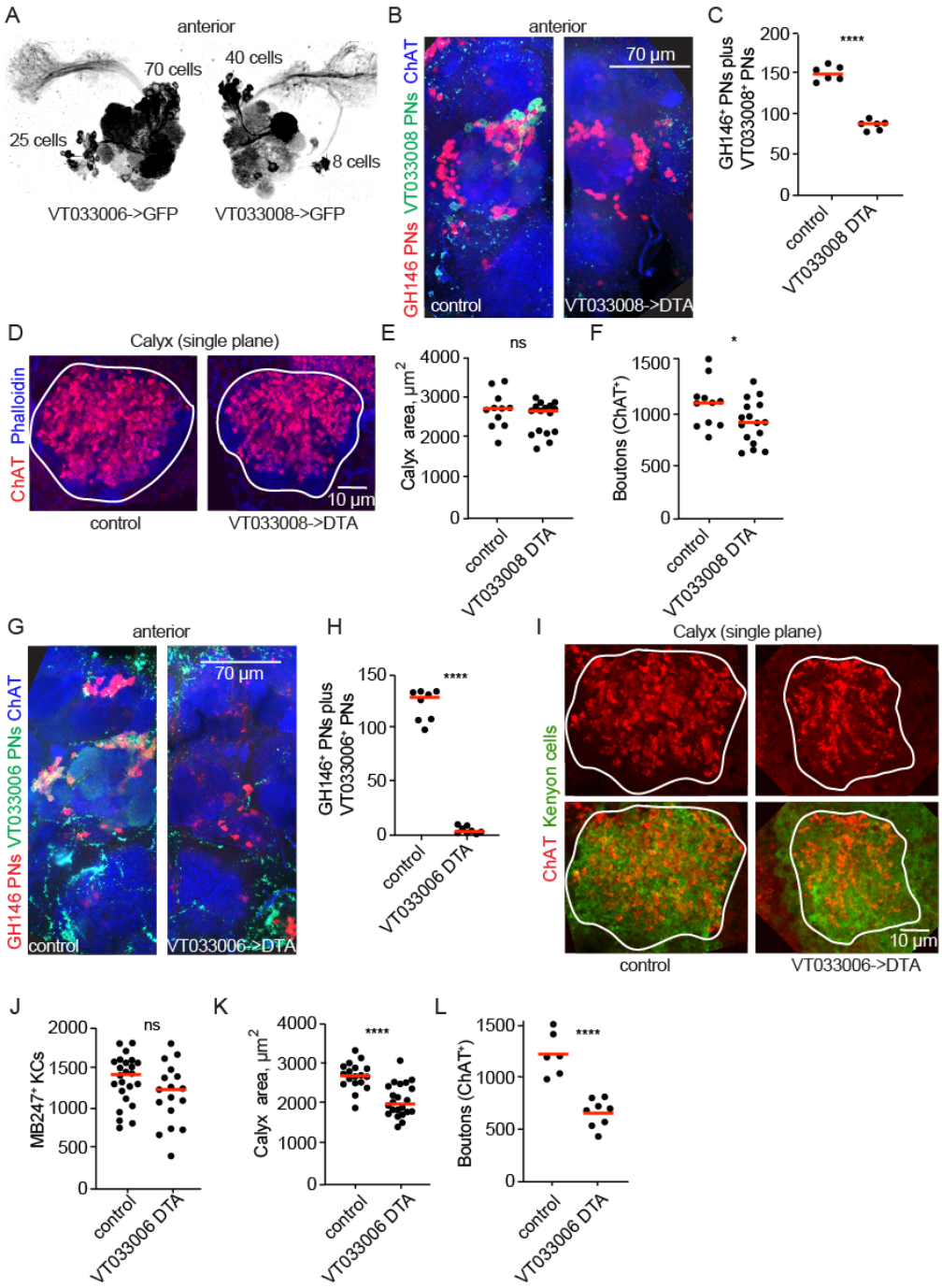

Figure 5: Projection neurons partially compensate for decreases in projection neuron population. (A) Maximum-intensity projections of two-photon stacks of brains with VT033006 (left) and VT033008 (right) driving GFP. (B) Maximum intensity projection of confocal stack of antennal lobes of control (left) and VT033008->DTA (right) brains. VT033008+ cells shown in green, GH146+ PNs, which partially overlap with VT033008+ PNs, shown in red. (C) Quantitation of PNs positive for GH146, VT033008, or both in control and VT033008->DTA brains. All VT033008+ cells are ablated in this genotype. Significance: unpaired t-test. Throughout this

figure, red horizonal bars represent medians. (D) Single confocal slice of control or VT033008->DTA calyx. Phalloidin signal shown in blue and ChAT+-boutons shown in red. (E, F) Quantification of calyx maximum cross-sectional area and bouton number in control and VT033008->DTA animals. Significance: unpaired t-test. (G) Maximum intensity projection of confocal stack of antennal lobes of control (left) and VT033006->DTA (right) brains. VT033006+ cells shown in green, GH146+ PNs, which partially overlap with VT033006+ PNs, shown in red. Green signals outside the antennal lobe in both conditions are autofluorescence. (H) Quantitation of PNs positive for GH146, VT033006, or both in control and VT033006->DTA brains. All VT033006+ cells are ablated in this genotype as well as most GH146+ PNs, even those that are not VT033006+ in the adult. Examination of ChAT+ neurites entering the calyx in VT033006->DTA brains suggests that up to 10 PNs may be labeled by neither VT033006 nor GH146, and that some of these may survive ablation. Significance: unpaired t-test. (I) Single confocal slice of control (left) or VT033006->DTA (right) calyx. KCs labeled using MB247-dsRed (shown green for continuity), ChAT+ boutons shown in red. (J-L) Quantification of the number of MB247+ KCs (J), calyx area (K), and ChAT+ boutons (L) in control or VT033006->DTA brains. Significance: unpaired t-test.

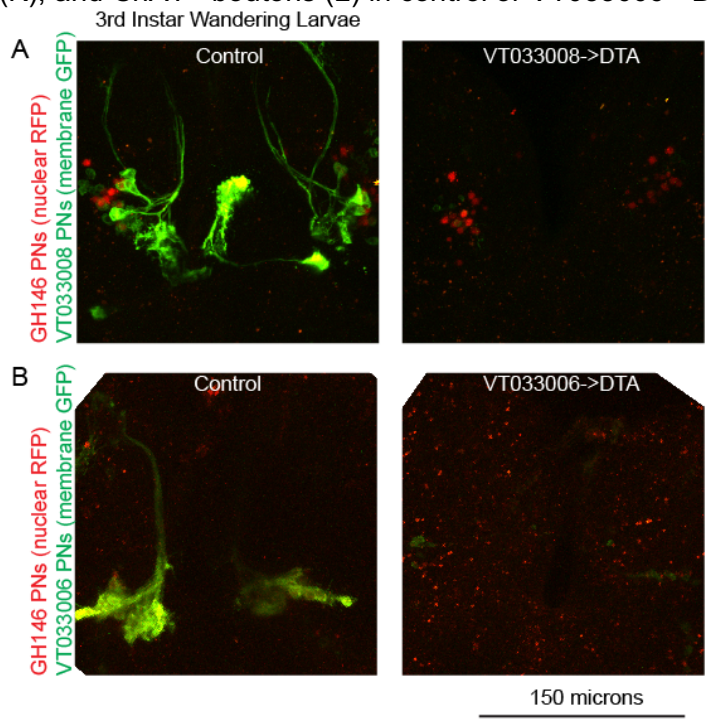

Figure 5-figure supplement 1. Maximum intensity projections of two photon stacks showing expression of VT033008-Gal4 (A) and VT033006-Gal4 (B) in third instar wandering larvae. Labeled cells are lost when these drivers are used to express DTA. The two samples in (A) were imaged and displayed using the same settings as one another, and the two samples in (B) were imaged and displayed using the same settings as one another. Red speckles in (B) are autofluorescence; GH146 signal is weak but detectable in nuclei of VT033006+ PNs in control but is lost in DTA samples. n=3-5 per genotype.

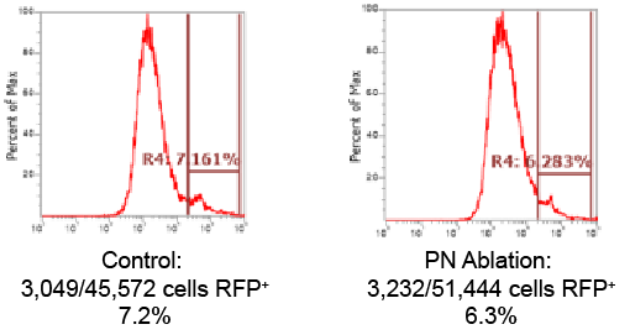

534

535 **Figure 5-figure supplement 2.** Number of KCs (MB247-dsRed, RFP+) detected in 3 pooled
536 control or 3 pooled VT033006->DTA brains dissociated and subjected to flow cytometry. Plots
537 depict cells already gated as singlets positive for a DNA dye, dyeCycle Violet. Representative of
538 two experiments.
539

540 **Projection neuron insufficiency has little effect on Kenyon cell claw number**

541 We expected that while KC claw number was largely invariant in the face of increases and de-
542 creases of the KC population, KCs would be forced to reduce their claw number when PN bou-
543 ton production was reduced by 50%, as in VT033006->DTA animals. We therefore compared
544 individual KCs in these animals versus controls. As different KC types produce different num-
545 bers of claws in wild type, we sought to simplify the analysis by labeling only a single KC type.
546 To do this, we targeted Texas red dextran dye electroporation to the tips of the mushroom body
547 α lobes, which are innervated by $\alpha\beta$ KCs (Figure 6A). This allowed us to label 1-12 KCs per ca-
548 lyx. We could discern discrete dye-labeled claws and somata in animals with eight or fewer KCs
549 labeled, and restricted our analyses to these samples (Figure 6B-D). For each hemisphere we
550 counted labeled somata and claws, generating one average value, claws per labeled KC, per
551 separable group of cells (Figure 6F). Surprisingly, despite 90% reduction in the number of PNs
552 and 50% reduction in their boutons, we observed no reduction in claw number per KC.
553

554 Do these enduring claws receive inputs? While labeled KCs in VT033006->DTA brains some-
555 times made clear contacts with spared PNs, as in Figure 6D, E, in other samples we also ob-
556 served KCs that avoided the one or few GH146-labeled, spared PNs (data not shown). Besides

557 PNs, GH146 labels an inhibitory neuron, APL, that innervates the mushroom body lobes and ca-
558 lyx. APL is presynaptic to KCs in the calyx, but innervates portions of KCs that are not claws
559 (Lin et al., 2014; Zheng et al., 2018). Labeled KCs in VT033006->DTA brains still formed con-
560 tacts with APL (Figure 6C).
561
562 A recent study in the *Drosophila* larval body wall found that neurons manipulated to produce ex-
563 cess dendrites can obtain input from atypical presynaptic partners (Tenedini et al., 2019). In wild
564 type animals, 10% of bouton inputs to Kenyon cells in the main (olfactory) calyx are from gusta-
565 tory or thermal modalities (Caron et al., 2013; Eichler et al., 2017; Frank et al., 2015; Kirkhart
566 and Scott, 2015; Zheng et al., 2018). It is possible that thermal or gustatory neurons projecting
567 to the calyx could have also expanded their production of boutons to make up for the losses of
568 olfactory PNs. We cannot yet determine whether the excess KC claws observed in this condition
569 get inputs from PN boutons, from APL, or from some other source. Nevertheless, these data
570 suggest that KCs are inflexible in their production of claws, even in the face of severe reduction
571 of their typical, favored presynaptic partners.

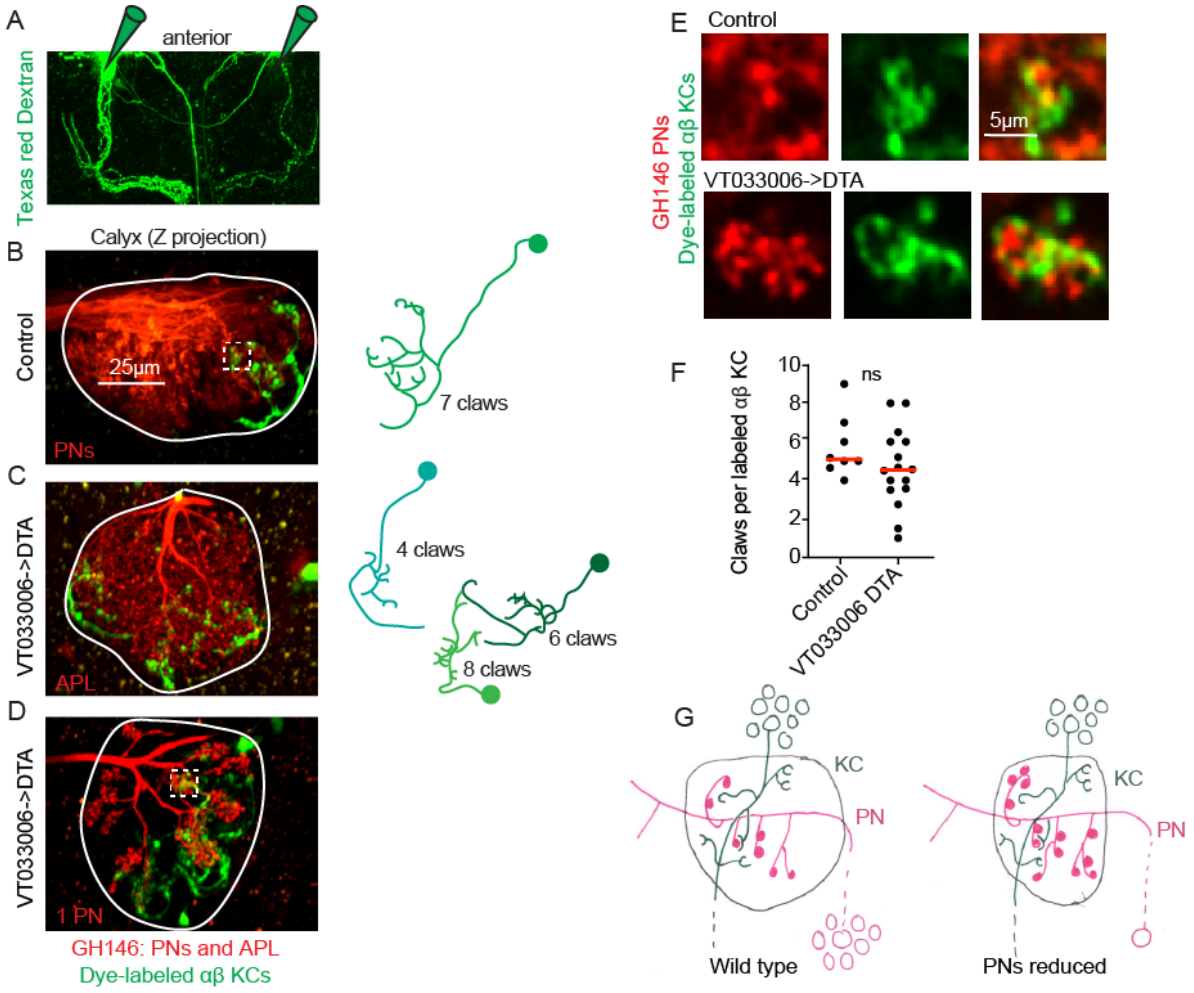

Figure 6: Kenyon cell claw number is unaffected by projection neuron bouton reduction. (A) Texas red dextran (colored green for continuity with green KCs in other figures) was electroporated into the tips of the mushroom body α lobes to allow specific targeting of αβ KCs. (B-D) Maximum intensity projections of two photon stacks of control (B) and VT033006->DTA (C, D) calyces. GH146, shown in red, labels PNs and APL. In control (B), APL is obscured by dense PN signal. In some VT033006->DTA hemispheres, as in (C), all GH146+ PNs were ablated, making APL signal apparent. In other VT033006->DTA hemispheres, as in (D), 1-2 GH146+ PNs remained. Texas red dextran dye diffusing from KC axons is shown in green. Diagrams show reconstructed anatomies of dye-labeled KCs. In (B), one KC with 7 claws is labeled. In C, three KCs with 4, 6, and 8 claws are labeled and can be spatially separated from one another. In D, 8 KCs are labeled and cannot be reconstructed. White boxes in (B) and (D) show regions magnified in (E). (E) Texas red dextran dye-labeled KC claws (green) wrapping GH146+ PN boutons (red) in control (top) and VT033006->DTA brains. (F) Quantification of claws per KC in control or VT033006->DTA samples. Each data point is the average number of claws per labeled KC for a spatially separated individual KC or small group of KCs. Significance: unpaired t-test. Red horizontal bars represent medians. (G) Model of the effect on calyx development of ablating large groups of PNs. Remaining PNs increase their production of boutons but cannot fully compensate for lost PNs, reducing the size of the calyx. KC claw numbers are similar to wild type; their source of innervation is unknown.

593 **Developmental plasticity preserves sparse odor coding despite perturbations to cell pop-**
594 **ulations**
595 The disparate and numerous strategies we used above to vary the ratio between PNs and KCs
596 all produced the same result, that PNs adjusted to changes in PN::KC ratio by altering their pre-
597 synaptic boutons, while the distribution of KC claw numbers changed little even when perturba-
598 tions to PNs were so severe as to prevent production of the normal bouton complement. This
599 finding suggests that developmental mechanisms prioritize the sparseness of olfactory inputs to
600 KCs, and might therefore preserve sparse odor coding and high-dimensional odor representa-
601 tions despite stark changes to the underlying circuit constituents. We therefore sought to ask
602 how KC odor responses were affected by perturbations to the PN::KC ratio.
603
604 We used OK107 to drive GCaMP6s expression in all KCs, and subjected animals to HU just af-
605 ter larval hatching. We then imaged KC somatic odor responses *in vivo* in 24 adult HU-treated
606 and 14 adult sham-treated animals. We observed robust odor responses in both conditions, with
607 8/28 sham-treated and 4/46 HU-treated calyces completely unresponsive. To identify HU-
608 treated hemispheres with reduced KC complement, following functional imaging we imaged the
609 anatomy of the calyx by two-photon or by immunostaining and confocal. Among ablated ani-
610 mals, we identified 14 of 46 imaged hemispheres in which calyces were clearly still present but
611 of reduced size, which we designate as “reduced-KC” calyces. We subjected these datasets
612 and 17 responsive controls to motion correction using Suite2p (Pachitariu et al., 2017). After
613 motion correction, seven sham and seven reduced KC calyces were sufficiently still to allow us
614 to define ROIs for individual somata. For each cell, we calculated peak change in fluorescence
615 following odor stimulus (Figure 7-source data 1). Example responses for sham-treated and re-
616 duced-KC calyces are shown in Figure 7A, B, C, Figure 7-figure supplement 1, and in Figure 7-
617 video 1, 2.
618

619 In order to compare response magnitudes across conditions, we first pooled all cells from each
620 condition and compared overall $\Delta f/f$ in response to each odor (Figure 7D). The distributions
621 were statistically indistinguishable between conditions for mineral oil (mechanosensory control),
622 ethyl acetate, and isobutyl acetate, and significantly different for benzaldehyde and methylcyclo-
623 hexanol. Using these aggregate responses, we set a threshold for "responsive" cells of 20% in-
624 crease in fluorescence over baseline, as we observed bifurcation of the cellwise response distri-
625 bution at this cutoff. Using these criteria, a median of ~50% of cells from sham calyces re-
626 sponded to ethyl acetate and isobutyl acetate, and ~20-30% of cells to benzaldehyde and
627 methylcyclohexanol (Figure 7E). These response rates are higher than has been reported with
628 GCaMP3 and GCaMP1 (Honegger et al., 2011; Wang et al., 2004), but correspond with spiking
629 response rates observed electrophysiologically (Murthy et al., 2008). We observed variation in
630 odor responses in both control and reduced-KC calyces; interindividual variation is expected
631 given the stochastic innervation of KCs by PNs.
632
633 We next compared the proportions of KCs per calyx responding to each odor between sham
634 and reduced-KC calyces. These distributions were statistically indistinguishable (Figure 7E). Fi-
635 nally, we asked how many odors each cell responded to (Figure 7F). In each condition, ~60% of
636 cells responded to 0 or 1 odors. Together, these findings suggest that the developmental plas-
637 ticity mechanisms operating to set the density of olfactory inputs to KCs preserve qualitatively
638 sparse KC odor responses when the KC population is experimentally reduced. Further experi-
639 ments will be required to assess quantitative effects of KC reduction on responses to odors that
640 typically stimulate fewer cells, like benzaldehyde and methylcyclohexanol.

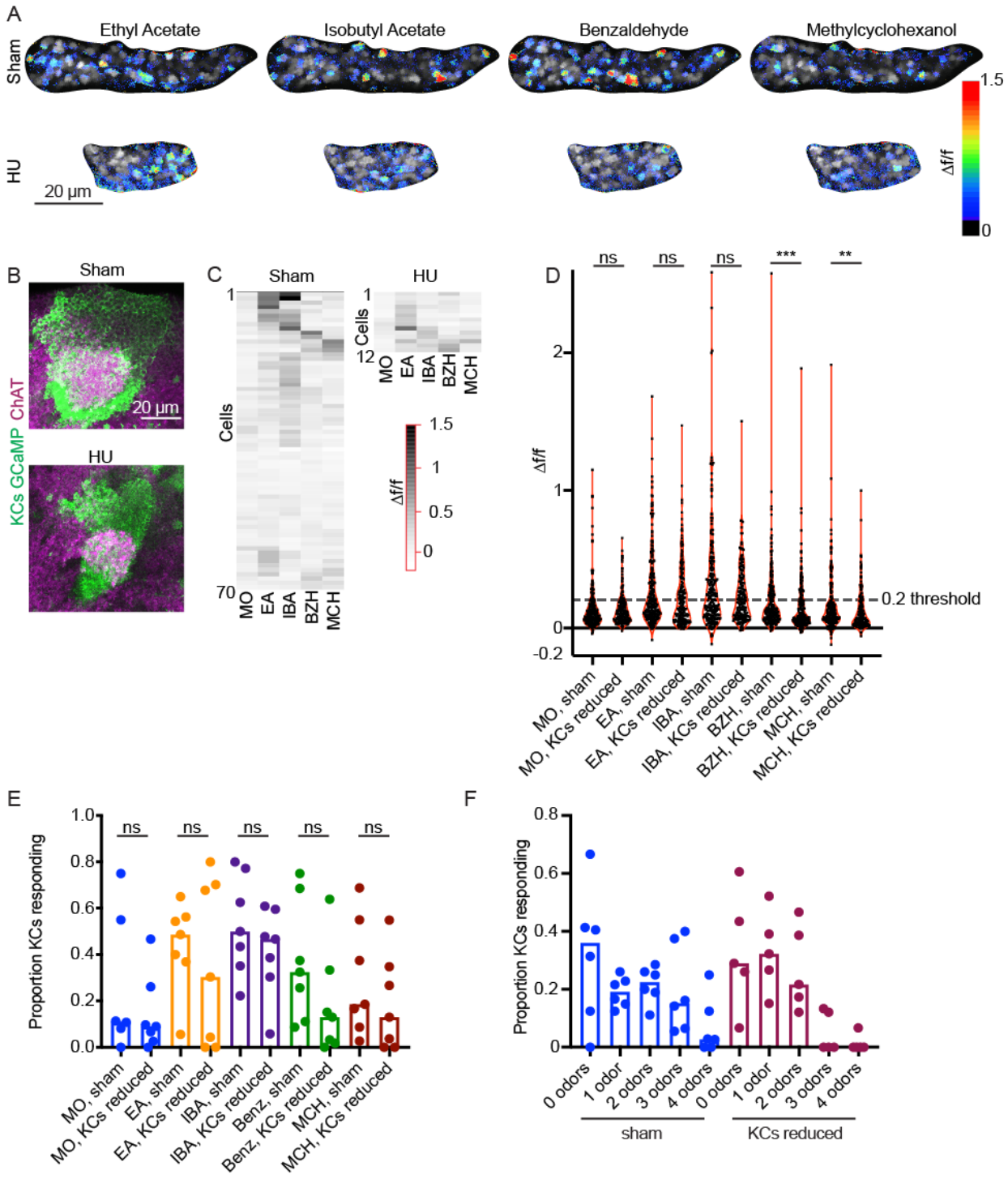

Figure 7: Odor responses in calyces with reduced KCs. (A) Example KC somatic odor responses in sham-treated hemisphere and HU-treated hemisphere with reduced KCs. (B) Post-imaging immunostaining showing calyces and KC somata of samples shown in (A). (C) Peak post-odor responses of individual KCs from samples shown in (A). Only cells that remained stable in their ROI for the whole stimulus panel are shown. Data was clustered by row such that cells with more similar odor responses are closer to one another. MO: Mineral oil (mechanosensory control), EA: Ethyl Acetate, IBA: Isobutyl Acetate, BZH: Benzaldehyde, MCH:

649 Methylcyclohexanol. (D) Peak odor responses of all cells, aggregated from all analyzed sam-
650 ples. Dashed line indicates 20% $\Delta f/f$ threshold. Significance: Mann-Whitney test. (E) Fraction of
651 cells in each sample responding to each odor at 20% $\Delta f/f$ threshold. Significance: unpaired t-
652 test. (F) For samples in which the same cells could be tracked across all odor presentations,
653 fraction of cells responding to 0, 1, or multiple odors is shown. Bar plots in (E, F) show medians.
654

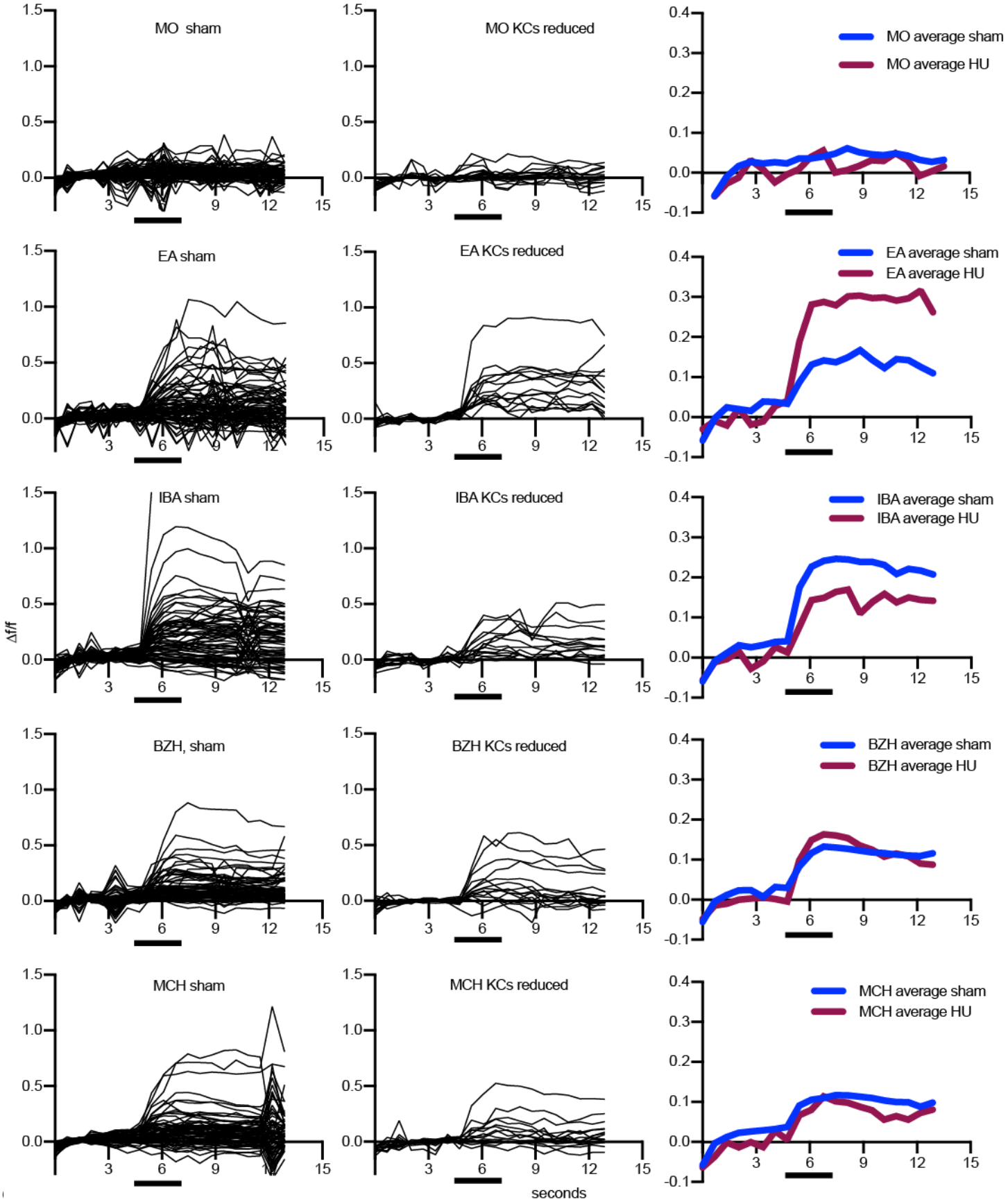
MO sham
MO KCs reduced
MO average sham
MO average HU
EA sham
EA KCs reduced
EA average sham
EA average HU
IBA sham
IBA KCs reduced
IBA average sham
IBA average HU
BZH, sham
BZH KCs reduced
BZH average sham
BZH average HU
MCH sham
MCH KCs reduced
MCH average sham
MCH average HU
Δf/f
seconds

Figure 7-figure supplement 1 Odor responses over time for cells shown in Figure 7A-C. x axes show seconds, y axes $\Delta f/f$. Black bars indicate odor delivery. Each black line is one cell, with graphs at right showing responses averaged across all cells of the sample. Each cell was normalized to average fluorescence in the 3-second period before stimulus onset. MO: Mineral oil (mechanosensory control), BZH: Benzaldehyde, EA: Ethyl Acetate, IBA: Isobutyl Acetate, MCH: Methylcyclohexanol. An example of a motion artifact can be seen in "MCH sham," around 12 seconds.

Discussion

Cerebellum-like architectures are found repeatedly in phylogenetically distinct organisms, suggesting that they have broad evolutionary utility. Yet the developmental production of sparseness, a key wiring feature allowing high-dimensional sensory representations, is not understood. Here, we have begun to investigate the development of sparse connectivity in the cerebellum-like associative learning center of insects, the mushroom body. By varying the ratio between presynaptic olfactory PNs and postsynaptic KCs, we find that connectivity density is set by KCs: KC claw number changes little across a wide range of PN::KC ratios, KC number predicts PN bouton number, and PNs exhibit wide variety in bouton number to satisfy KC demands. As described below, we expect that this strategy for generating connectivity density would preserve sparseness in KC inputs across developmental time and upon evolutionary changes in cell repertoires and thus maintain the olfactory coding function of the mushroom body over a range of conditions.

Implications for development: Different projection neuron::Kenyon cell ratios across developmental stages

For many animals, brain development continues while juveniles are already living freely--searching for food, navigating, and learning about the environment. Developmental transitions in brain structure are particularly stark in holometabolous insects, who build the brain twice. In flies, neurons generated during embryonic and early larval stages wire the larval nervous system. These circuits support larval behaviors, while neural stem cells continue to generate additional neurons that will be used to build the adult circuit. In keeping with this, the ratio between

686 PNs and KCs in the larval olfactory circuit is starkly different from the adult: 21 embryonically-
687 born PNs wire to early-born KCs to construct the larval mushroom body (Eichler et al., 2017;
688 Masuda-Nakagawa et al., 2005; Ramaekers et al., 2005). Connections among these popula-
689 tions dissolve in early pupae, and are then re-wired during pupal development (Lee et al., 1999;
690 Marin et al., 2005), joined by ~100 more larvally-born PNs, and >1000 more KCs per hemi-
691 sphere that continue to be born until immediately before adult eclosion.
692
693 The 21 PNs in the early larva connect to 75 KCs, a 1:3 ratio, while in the adult, 150 PNs connect
694 to 2000 KCs, a 1:10 ratio. (Eichler et al., 2017; Zheng et al., 2018). We found that unlike cells in
695 many other systems, including the vertebrate cerebellum, PNs and KCs did not rely on each
696 other for survival signals (Fan et al., 2001). This may be due to the constantly changing ratio be-
697 tween these cell types across developmental time. Instead, setting connectivity density cell-au-
698 tonomously in KCs could allow KCs to obtain the appropriate number of inputs at the different
699 life stages of the animal, when cellular constituents are very different from one another. Simi-
700 larly, while PN neurogenesis ceases well before PNs and KCs begin to contact one another in
701 the pupa, we estimate that ~10% of KCs are born after PN:KC synapsis has already initiated
702 (Muthukumar et al., 2014). Strict, cell-autonomous dendrite structuring and flexible PN bouton
703 production could together ensure that late-born KCs obtain the inputs appropriate to support
704 coding.
705
706 **Implications for coding: Balancing projection neuron representations across the calyx**
707 Olfactory PNs of different types are specified in a predictable temporal order, have characteristic
708 numbers of boutons, and overlap in their innervation of the calyx (Lai et al., 2008; Yu et al.,
709 2010; Zheng et al., 2018). Differences in bouton number across different PNs allow different
710 odor channels to be differentially represented in the calyx and in KC odor responses (Caron et
711 al., 2013; Honegger et al., 2011; Murthy et al., 2008). Several classes of PNs also differ in

712 number between the sexes (Grabe et al., 2016). While PNs changed their individual bouton rep-
713 ertoires in response to changes in cell repertoires, we found that to some extent, the represen-
714 tation level of different PNs in the calyx was preserved. For example, in Figure 2F and Figure 2-
715 figure supplement 2, we show the effect of reducing KC number on bouton production by the
716 VM6 PN and 42D01 PNs. While each population of PNs reduced individual bouton number in
717 this condition, they retained their typical relative representation. The VM6 PN reduced its bou-
718 tons from 10 to 5, while the 42D01 PNs decreased their boutons from 4 to 2. Similarly, in Figure
719 4, we expanded the PN population by inducing ectopic PN neuroblast duplication. In these ex-
720 periments, we mainly observed amplification of the ventrolateral clone. We found that individual
721 anterodorsal VM6 cells did not scale down their boutons when the ventrolateral PN clone ex-
722 panded, but only when VM6 itself was duplicated. Again, this could maintain the relative wild
723 type representations of different odor channels in the calyx. A recent analysis suggests that the
724 spontaneous activity of different ORs correlates with number of boutons representing that odor
725 channel in the calyx (Kennedy, 2019). One possible model for how PNs scale to KC numbers
726 while maintaining their relative representations in the calyx is thus that KC number limits total
727 bouton number across all PNs, while allocation of these boutons to individual PNs is determined
728 by activity-based competition among PN types.
729
730 **Implications for coding: Maximizing dimensionality of odor representations**
731 Qualitative aspects of sparse coding in the mushroom body appear robust to severe perturba-
732 tions to the circuit. Alternative developmental compensatory mechanisms would be much less
733 likely to preserve sparse coding. For example, we increased the ratio of PNs to KCs in two
734 ways, by increasing the number of PNs and by decreasing the number of KCs. In both cases,
735 PNs dialed down their bouton number, making 25-50% of the boutons they make in wild type.
736 This allowed the KCs to receive their typical number of inputs. If in contrast bouton number was
737 rigid and claw number flexible, in these cases KCs would have expanded their claw production

738 2-4 fold to innervate all the incoming PN boutons. Individual KCs with e.g. 20 instead of 5 claws
739 would receive input from ~40% of glomeruli, increasing the overlap in tuning across different
740 KCs and degrading the ability of the network to distinguish different stimuli from one another
741 (Litwin-Kumar et al., 2017).
742
743 In two other cases, we increased the ratio of KCs to PNs, by increasing the number of KCs and
744 by decreasing the number of PNs. Again, KCs retained their typical claw number. If instead PNs
745 had maintained a static production of boutons while KCs had adjusted their claw production,
746 KCs would receive very few inputs. While increasing the number of inputs per KC is theorized to
747 reduce dimensionality of odor responses by making different KCs more similar to one another,
748 decreasing the number of inputs per KC is theorized to reduce dimensionality by reducing the
749 number of different possible KC input combinations (Litwin-Kumar et al., 2017). That this sweet
750 spot maximizing dimensionality, ~5 inputs per cells, is programmed into KC identity testifies to
751 the evolutionary importance of maintaining connectivity density in associative brain centers that
752 rely on combinatorial coding.
753
754 **Implications for evolution: The potential for mushroom body function despite perturba-**
755 **tions**
756 The olfactory receptors are the largest insect gene family and have been subject to frequent and
757 extreme gains and losses in many clades. Similarly, brain centers devoted to learning are radi-
758 cally different across species, as exemplified by the diversity in KC repertoire across arthropods
759 (Strausfeld et al., 2009). In order to acquire a novel olfactory circuit, many different evolutionary
760 changes are required: A new receptor must evolve, an OSN type that uniquely expresses the
761 receptor needs to arise, that OSN needs to synapse onto PNs, and a new PN type and new
762 glomerulus must arise. For these events to accrue over time, each individual change must be
763 compatible with continued circuit function and olfactory behavior. While development of a

764 dedicated circuit that assigns an innate meaning to a newly-detectable odor would require many
765 further changes, the signal could add to fitness immediately through representation in the mush-
766 room body.
767
768 We have described two mechanisms of developmental robustness that maintain coherent
769 mushroom body wiring in the face of a broad range of phenotypic alterations. First, we observe
770 that olfactory PNs can adjust to gain and loss of PNs while maintaining the balance of odor
771 channel representations in the calyx. Plastic development of PN presynaptic sites that makes
772 room for additional players in the repertoire would allow immediate access of evolutionarily ex-
773 panded PNs to the calyx and the use of their signals for olfactory learning, thus making time for
774 the evolution of hardwired circuits for innate interpretations. Second, we show here that devel-
775 opmental programs wiring the calyx can accommodate variation in KC number from at least ¼
776 to 2-fold the endogenous complement. Again, this flexibility could support continued MB function
777 on the path to the evolution of mushroom body innovations. Future experiments will ask how KC
778 claw number is developmentally programmed, and what mechanisms operate in olfactory PNs
779 to allow them to tailor bouton production to the KC repertoire.
780
781 **Acknowledgements**
782 We thank the Bloomington Drosophila Stock Center, Yoshi Aso, and Tzumin Lee for providing
783 fly strains; Vanessa Ruta for intellectual and material support during the early phases of this
784 project; Isaac Levine, Shiloh Boosamra, Noella Holmer, Joseph Carter, and James Harrison for
785 technical assistance; Shyama Nandakumar for help with flow cytometry experiments; Christina
786 May, Swathi Yadlapalli, Ari Zolin, Yoshi Aso, Ashok Litwin-Kumar, Laura Buttitta, and members
787 of the Cheng-Yu Lee lab for experimental advice and discussion; and Cathy Collins, Monica
788 Dus, Rich Hume, Vanessa Ruta, and members of the E.J.C lab for comments on the manu-
789 script. This work was supported by the Simons Fellowship of the Helen Hay Whitney Foundation

790 to E.J.C. E.J.C. is the Rita Allen Foundation Milton Cassel Scholar and is supported by the Al-
791 fred P. Sloan Foundation Award, and by a Neuroscience Scholar Award and start-up funds from
792 the University of Michigan.

793

794 **Competing Interests:** The authors declare no competing interests.

795

796 **Materials and Methods**
797

Key Resources Table				
Reagent type (species) or resource	**Designation**	**Source or reference**	**Identifiers**	**Additional information**
gene (*Drosophila melanogaster*)	mud		FLYB: FBgn0002873	
genetic reagent (*Drosophila melanogaster*)	GH146^{Gal4} (II)	Bloomington Drosophila Stock Center	BDSC 30026	(Stocker et al., 1997)
genetic reagent (*Drosophila melanogaster*)	10XUAS-IVS-myr::tdTomato (attp40)	Bloomington Drosophila Stock Center	BCSC 32222	(Pfeiffer et al., 2012)
genetic reagent (*Drosophila melanogaster*)	MB247-LexAVP16 (III)	Scott Waddell, University of Oxford		(Pitman et al., 2011)
genetic reagent (*Drosophila melanogaster*)	LexAop-CD2-GFP (III)	Bloomington Drosophila Stock Center	BDSC 66544	(Lai and Lee, 2006)
genetic reagent	GH146^{LexA} (II)	Tzumin Lee, Janelia Farms		(Lai et al., 2008)

(*Drosophila melanogaster*)		Research Campus		
genetic reagent (*Drosophila melanogaster*)	lexAop-mRFP-nls (II)	Bloomington Drosophila Stock Center	BDSC 29956	Gunter Merdes
genetic reagent (*Drosophila melanogaster*)	58F02-Gal4 (attp2)	Bloomington Drosophila Stock Center	BDSC 39186	(Jenett et al., 2012)
genetic reagent (*Drosophila melanogaster*)	UAS-GCaMP6s (attp40)	Bloomington Drosophila Stock Center	BDSC 42746	(Akerboom et al., 2012)
genetic reagent (*Drosophila melanogaster*)	UAS-GCaMP6s (VK0005)	Bloomington Drosophila Stock Center	BDSC 42749	(Akerboom et al., 2012)
genetic reagent (*Drosophila melanogaster*)	MB247-DsRed (II)	André Fiala		(Riemensperger et al., 2005)
genetic reagent (*Drosophila melanogaster*)	71D09-Gal4 (attp2)	Bloomington Drosophila Stock Center	BDSC 39584	(Jenett et al., 2012)
genetic reagent (*Drosophila melanogaster*)	UAS-CD8GFP (III)	Bloomington Drosophila Stock Center	BDSC 5130	(Lee and Luo, 1999)
genetic reagent (*Drosophila melanogaster*)	42D01-Gal4 (attp2)	Bloomington Drosophila Stock Center	BDSC 50152	(Jenett et al., 2012)
genetic reagent (*Drosophila melanogaster*)	UAS-C3PA (II)	Vanessa Ruta, Rockefeller University		(Ruta et al., 2010)

genetic reagent (*Drosophila melanogaster*)	UAS-C3PA (III)	Vanessa Ruta, Rockefeller University		(Ruta et al., 2010)
genetic reagent (*Drosophila melanogaster*)	60A10-LexA (attp40)	Bloomington Drosophila Stock Center	BDSC 52821	Pfeiffer, Rubin LexA Collection
genetic reagent (*Drosophila melanogaster*)	LexAop-tdTomato.Myr (su(Hw)attp5)	Bloomington Drosophila Stock Center	BDSC 56142	(Chen et al., 2014)
genetic reagent (*Drosophila melanogaster*)	89B01-Gal4 (attp2)	Bloomington Drosophila Stock Center	BDSC 40541	(Jenett et al., 2012)
genetic reagent (*Drosophila melanogaster*)	13XLexAop2-IVS-Syn21-mC3PA-GFP-p10 (attp2)	Gerry Rubin, Janelia Farms Research Campus		(Pfeiffer et al., 2012)
genetic reagent (*Drosophila melanogaster*)	GH146^{QF}, QUAS-mtdTomato-3xHA (II)	Bloomington Drosophila Stock Center	BDSC 30037	(Potter et al., 2010)
genetic reagent (*Drosophila melanogaster*)	UAS-mud-RNAi (attp2)	Bloomington Drosophila Stock Center	BDSC 35044	(Perkins et al., 2015)
genetic reagent (*Drosophila melanogaster*)	OK107^{Gal4} (IV)	Bloomington Drosophila Stock Center	BDSC 854	(Connolly et al., 1996)
genetic reagent (*Drosophila melanogaster*)	P(caryP) (attp2)	Bloomington Drosophila Stock Center	BDSC 36303	(Perkins et al., 2015)
genetic reagent (*Drosophila melanogaster*)	P(caryP) (attp40)	Bloomington Drosophila Stock Center	BDSC 36304	(Perkins et al., 2015)

genetic reagent (*Drosophila melanogaster*)	MZ19^{QF} (II)	Bloomington Drosophila Stock Center	BDSC 41573	(Hong et al., 2012)
genetic reagent (*Drosophila melanogaster*)	QUAS-mtdTomato-3xHA (II)	Bloomington Drosophila Stock Center	BDSC 30004	(Potter et al., 2010)
genetic reagent (*Drosophila melanogaster*)	41C07-LexA (attp40)	Bloomington Drosophila Stock Center	BDSC 54791	Pfeiffer, Rubin LexA Collection
genetic reagent (*Drosophila melanogaster*)	89B01-LexA (attp40)	Bloomington Drosophila Stock Center	BDSC 54380	Pfeiffer, Rubin LexA Collection
genetic reagent (*Drosophila melanogaster*)	71D09-LexA (attp40)	Bloomington Drosophila Stock Center	BDSC 54931	Pfeiffer, Rubin LexA Collection
genetic reagent (*Drosophila melanogaster*)	LexAop-SPA-T2A-SPA (II)	n/a		(Clowney et al., 2015)
genetic reagent (*Drosophila melanogaster*)	44F03-Gal4 (attp2)	Tzumin Lee, Janelia Farms Research Campus		(Awasaki et al., 2014)
genetic reagent (*Drosophila melanogaster*)	VT033006-Gal4 (attp2)	Yoshi Aso, Janelia Farms Research Campus		(Kvon et al., 2014)
genetic reagent (*Drosophila melanogaster*)	VT033008-Gal4 (attp2)	Yoshi Aso, Janelia Farms Research Campus		(Kvon et al., 2014)
genetic reagent (*Drosophila melanogaster*)	UAS-DTA (UAS-Cbbeta\DT-A.I)[18] (II)	Bloomington Drosophila Stock Center	BDSC 25039	(Han et al., 2000)

antibody	ChAT (mouse mono-clonal)	Developmen-tal Studies Hybridoma Bank	9E10	(1:200)
antibody	DsRed (rabbit poly-clonal)	Clontech	632496	(1:500-1:1000)
antibody	GFP (sheep poly-clonal)	Bio-Rad	4745-1051	(1:250-1:1000)
antibody	GFP (chicken poly-clonal)	Gift from Dawen Cai	n/a	(1:5000)
antibody	Alexa 488 anti-mouse (goat poly-clonal)	Fisher	A11029	(1:500)
antibody	Alexa 647 anti-mouse (goat poly-clonal)	Fisher	A21236	(1:500)
antibody	Alexa 488 anti-sheep (donkey pol-yclonal)	Fisher	A11015	(1:500)
antibody	Alexa 488 anti-chicken (goat poly-clonal)	Fisher	A11039	(1:500)
antibody	Alexa 568 anti-rab-bit (goat polyclonal)	Fisher	A11036	(1:500)
chemical compound, drug	Texas Red Dextran	Fisher	D3328	

chemical compound, drug	Alexa 568 Phalloidin	Fisher	A12380	
chemical compound, drug	Schneider's medium	Sigma	S0146	
chemical compound, drug	Paraformaldehyde	EMS	15710	
chemical compound, drug	Hydroxyurea	Sigma	H8627	
chemical compound, drug	Benzaldehyde	Sigma	418099	
chemical compound, drug	Isobutyl acetate	Sigma	537470	
chemical compound, drug	Ethyl acetate	Sigma	270989	
chemical compound, drug	Methylcyclohexanol	Sigma		
peptide, recombinant protein	Collagenase	Sigma		
software, algorithm	Suite2p	(Pachitariu et al., 2017)		
other	Duck EZ Start Packaging tape	Office Depot	511879	
other	UV Glue	Loctite	3106	
other	JAXMAN 365nm Flashlight	Amazon	B077GPXBK1	

other	Electra Waxer	Almore	66000	
other	Gulfwax Paraffin	Grocery store	C0130	
other	hair	self		

Flies: Flies were maintained on cornmeal-molasses ("R") food (Lab Express, Ann Arbor, MI) in a humidified incubator at 25C on a 12:12 light:dark cycle.

Alleles and Sources:

Allele	**Source**	**Reference**
GH146^{Gal4} (II)	BL 30026	(Stocker et al., 1997)
10XUAS-IVS-myr::tdTomato (attp40)	BL 32222	(Pfeiffer et al., 2012)
MB247-LexAVP16 (III)	Scott Waddell, University of Oxford	(Pitman et al., 2011)
LexAop-CD2-GFP (III)	BL 66544	(Lai and Lee, 2006)
GH146^{LexA} (II)	Tzumin Lee, Janelia Farms Research Campus	(Lai et al., 2008)
lexAop-mRFP-nls (II)	BL 29956	Gunter Merdes
58F02-Gal4 (attp2)	BL 39186	(Jenett et al., 2012)
UAS-GCaMP6s (attp40)	BL 42746	(Akerboom et al., 2012)
UAS-GCaMP6s (VK0005)	BL 42749	(Akerboom et al., 2012)
MB247-DsRed (II)	André Fiala	(Riemensperger et al., 2005)
71D09-Gal4 (attp2)	BL 39584	(Jenett et al., 2012)
UAS-CD8GFP (III)	BL 5130	(Lee and Luo, 1999)
42D01-Gal4 (attp2)	BL 50152	(Jenett et al., 2012)
UAS-C3PA (II)	Vanessa Ruta, Rockefeller University	(Ruta et al., 2010)
UAS-C3PA (III)	Vanessa Ruta, Rockefeller University	(Ruta et al., 2010)
60A10-LexA (attp40)	BL 52821	Pfeiffer, Rubin LexA Collection
LexAop-tdTomato.Myr (su(Hw)attp5)	BL 56142	(Chen et al., 2014)
89B01-Gal4 (attp2)	BL 40541	(Jenett et al., 2012)
13XLexAop2-IVS-Syn21-mC3PA-GFP-p10 (attp2)	Gerry Rubin, Janelia Farms Research Campus	(Pfeiffer et al., 2012)
GH146^{QF}, QUAS-mtdTomato-3xHA (II)	BL30037	(Potter et al., 2010)
UAS-mud-RNAi (attp2)	BL35044	(Perkins et al., 2015)
OK107^{Gal4} (IV)	BL 854	(Connolly et al., 1996)
P(caryP) (attp2)	BL36303	(Perkins et al., 2015)
P(caryP) (attp40)	BL36304	(Perkins et al., 2015)
MZ19^{QF} (II)	BL41573	(Hong et al., 2012)

QUAS-mtdTomato-3xHA (II)	BL 30004	(Potter et al., 2010)
41C07-LexA (attp40)	BL 54791	Pfeiffer, Rubin LexA Collection
89B01-LexA (attp40)	BL 54380	Pfeiffer, Rubin LexA Collection
71D09-LexA (attp40)	BL 54931	Pfeiffer, Rubin LexA Collection
LexAop-SPA-T2A-SPA (II)	n/a	(Clowney et al., 2015)
44F03-Gal4 (attp2)	Tzumin Lee, Janelia Farms Research Campus	(Awasaki et al., 2014)
VT033006-Gal4 (attp2)	Yoshi Aso, Janelia Farms Research Campus	(Kvon et al., 2014)
VT033008-Gal4 (attp2)	Yoshi Aso, Janelia Farms Research Campus	(Kvon et al., 2014)
UAS-DTA (UAS-Cbbeta\DT-A.I)[18] (II)	BL 25039	(Han et al., 2000)

Genotypes were as follows:

Figure 1, Figure 1-figure supplement 1	GH146^{Gal4}, 10XUAS-IVS-myr::tdTomato/CyO; MB247-lexA, lexAop-CD2-GFP/TM2
Figure 1-figure supplement 2	GH146^{LexA}, lexAop-mRFP-nls / P(caryP)attp40; VT033006-Gal4, UAS-CD8GFP/+
Figure 2A-E	GH146^{LexA}, lexAop-mRFP-nls/CyO; 58F02-Gal4, UAS-GCaMP6s/TM2
Figure 2F-H	MB247-DsRed/CyO; 71D09-Gal4, UAS-CD8GFP/"
Figure 2I	60A10-LexA, LexAop-tdTomato.Myr/CyO; 58F02-Gal4, UAS-C3PA/"
Figure 2J, K	GH146^{Gal4}, 10XUAS-IVS-myr::tdTomato /CyO; MB247-lexA, 13XLexAop2-IVS-Syn21-mC3PA-GFP-p10/"
	60A10-LexA, LexAop-tdTomato.Myr /CyO; 58F02-Gal4, UAS-C3PA/"
Figure 2-figure supplement 1	GH146^{LexA}, lexAop-mRFP-nls/CyO; 58F02-Gal4, UAS-GCaMP6s/TM2
Figure 2-figure supplement 2	MB247-DsRed/CyO; 42D01-Gal4, UAS-C3PA/"
Figure 2-figure supplement 3A, B	GH146^{Gal4}, 10XUAS-IVS-myr::tdTomato /CyO; MB247-lexA, 13XLexAop2-IVS-Syn21-mC3PA-GFP-p10/"
Figure 2-figure supplement 3C, D	GH146^{Gal4}, 10XUAS-IVS-myr::tdTomato /CyO; MB247-lexA, 13XLexAop2-IVS-Syn21-mC3PA-GFP-p10/"
	60A10-LexA, LexAop-tdTomato.Myr /CyO; 89B01-Gal4, UAS-C3PA/"

Figure 3A-C	GH146^{QF}, QUAS-mtdTomato-3xHA /+; UAS-CD8GFP/UAS-mud-RNAi; OK107^{Gal4}/+
	GH146^{QF}, QUAS-mtdTomato-3xHA /+; UAS-CD8GFP/ P(caryP)attp2; OK107^{Gal4}/+

Figure 3D-G	MZ19^{QF}, QUAS-mtdTomato-3xHA /Bl; UAS-mud-RNAi/TM2 or TM6B; OK107^{Gal4}/+
	MZ19^{QF}, QUAS-mtdTomato-3xHA /Bl; P(caryP)attp2/TM2 or TM6B; OK107/+
Figure 3H	71D09-LexA, LexAop-tdTomato.Myr /Bl; UAS-mud-RNAi/TM2; OK107 ^{Gal4}/+
	71D09-LexA, LexAop-tdTomato.Myr /Bl; P(caryP)attp2/TM2; OK107 ^{Gal4}/+
Figure 3I	UAS-C3PA/+; UAS-C3PA/ UAS-mud-RNAi; OK107^{Gal4}/+
	UAS-C3PA/+; UAS-C3PA/ P(caryP)attp2; OK107^{Gal4}/+
Figure 3J, K	UAS-C3PA/+; UAS-C3PA/ UAS-mud-RNAi; OK107^{Gal4}/+
	UAS-C3PA/+; UAS-C3PA/ P(caryP)attp2; OK107^{Gal4}/+
	UAS-C3PA/41C07-LexA, LexAop-tdTomato.Myr; UAS-C3PA/ UAS-mud-RNAi; OK107^{Gal4}/+
	UAS-C3PA/41C07-LexA, LexAop-tdTomato.Myr; UAS-C3PA/ P(caryP)attp2; OK107 ^{Gal4}/+
	UAS-C3PA/89B01-LexA, LexAop-tdTomato.Myr; UAS-C3PA/ UAS-mud-RNAi; OK107 ^{Gal4}/+
	UAS-C3PA/89B01-LexA, LexAop-tdTomato.Myr; UAS-C3PA/ P(caryP)attp2; OK107 ^{Gal4}/+
Figure 3-figure supplement 1	41C07-LexA, LexAop-tdTomato.Myr /UAS-C3PA; UAS-mud-RNAi 35044/UAS-C3PA; OK107 ^{Gal4}/+
	41C07-LexA, LexAop-tdTomato.Myr /UAS-C3PA; P(caryP)attp2/UAS-C3PA; OK107 ^{Gal4}/+
Figure 4A-I	GH146^{LexA}, LexAop-SPA-T2A-SPA /+; 44F03-Gal4/ UAS-mud-RNAi
	GH146^{LexA}, LexAop-SPA-T2A-SPA /+; 44F03-Gal4/ P(caryP)attp2
Figure 4J-M	GH146^{LexA}, LexAop-SPA-T2A-SPA /MZ19^{QF}, QUAS-mtdTomato-3xHA; 44F03-Gal4/ UAS-mud-RNAi
	GH146^{LexA}, LexAop-SPA-T2A-SPA /MZ19^{QF}, QUAS-mtdTomato-3xHA; 44F03-Gal4/ P(caryP)attp2
	MZ19^{QF}, QUAS-mtdTomato-3xHA /+; 44F03-Gal4/ UAS-mud-RNAi
	MZ19^{QF}, QUAS-mtdTomato-3xHA /+; 44F03-Gal4/ P(caryP)attp2
Figure 4-figure supplement 1A, B	GH146^{LexA}, LexAop-SPA-T2A-SPA /+; 44F03-Gal4/ UAS-mud-RNAi
	GH146^{LexA}, LexAop-SPA-T2A-SPA /+; 44F03-Gal4/ P(caryP)attp2
Figure 4-figure supplement 1D-F	71D09-LexA, LexAop-tdTomato.Myr /+; 44F03-Gal4/ UAS-mud-RNAi
	71D09-LexA, LexAop-tdTomato.Myr /+; 44F03-Gal4 P(caryP)attp2
Figure 5A	CyO/+; VT033006-Gal4/UAS-CD8GFP
	CyO/+; VT033008-Gal4/UAS-CD8GFP
Figure 5B, C	GH146^{LexA}, lexAop-mRFP-nls /UAS-DTA; VT033008-Gal4, UAS-CD8GFP/+
	GH146^{LexA}, lexAop-mRFP-nls / P(caryP)attp40; VT033008-Gal4, UAS-CD8GFP/+
Figure 5D-F	UAS-DTA/+; VT033008-Gal4/TM6B

	UAS-DTA/+; P(caryP)attp2/TM6B

809

Figure 5G, H	GH146^{LexA}, lexAop-mRFP-nls / UAS-DTA; VT033006-Gal4, UAS-CD8GFP/+
	GH146^{LexA}, lexAop-mRFP-nls / P(caryP)attp40; VT033006-Gal4, UAS-CD8GFP/+
Figure 5I-L	MB247-DsRed/ UAS-DTA; VT033006-Gal4, UAS-CD8GFP/+
	MB247-DsRed/+; VT033006-Gal4, UAS-CD8GFP/+
Figure 5-figure supplement 1A	GH146^{LexA}, lexAop-mRFP-nls /UAS-DTA; VT033008-Gal4, UAS-CD8GFP/+
	GH146^{LexA}, lexAop-mRFP-nls / CyO; VT033008-Gal4, UAS-CD8GFP/+
Figure 5-figure supplement 1B	GH146^{LexA}, lexAop-mRFP-nls / UAS-DTA; VT033006-Gal4, UAS-CD8GFP/+
	GH146^{LexA}, lexAop-mRFP-nls / CyO; VT033006-Gal4, UAS-CD8GFP/+
Figure 5-figure supplement 2	MB247-DsRed/ UAS-DTA; VT033006-Gal4, UAS-CD8GFP/+
	MB247-DsRed/+; VT033006-Gal4, UAS-CD8GFP/+
Figure 6	GH146^{LexA}, LexAop-SPA-T2A-SPA / UAS-DTA; VT033006-Gal4/+
	GH146^{LexA}, LexAop-SPA-T2A-SPA / P(caryP)attp40; VT033006-Gal4/+
Figure 7, Figure 7-figure supplement 1, Figure 7-video 1, 2	UAS-GCaMP6s/UAS-GCaMP6s; UAS-GCaMP6s/UAS-GCaMP6s; OK107^{Gal4}/ OK107^{Gal4} or +

810
811 *HU ablation:* Protocol was adapted from Sweeney et al (Sweeney et al., 2012). Briefly, we set
812 up large populations of flies in cages two days prior to ablation and placed a 35 or 60mm grape
813 juice agar plate (Lab Express, Ann Arbor, MI) in the cage with a dollop of goopy yeast. One day
814 prior to the ablation, we replaced the grape juice/yeast plate with a new grape juice/yeast plate.
815 On the morning of the ablation, we removed the plate from the cage one hour after lights-on and
816 discarded the yeast puck and any hatched larvae on the agar. We then monitored the plate for
817 up to four hours, until many larvae had hatched. Larvae were washed off the plate using a su-
818 crose solution, and eggs were discarded. Larvae were then strained in coffee filters, and sub-
819 merged in hydroxyurea (Sigma, H8627) in a yeast:AHL mixture, or sham mixture without HU.
820 Ablation conditions were as follows:
821
822 Figure 1: 10mg/mL or 5mg/mL, 4 hours
823 Figure 2A-E: 10mg/mL, 1 hour
824 Figure 2F-K, Figure 2-figure supplement 2, 3: 10mg/mL, 1 hour; 3 or 5 mg/mL, 4 hours
825 Figure 7, Figure 7-figure supplement 1: 10mg/mL, 1 hour
826
827 Larvae were then strained through coffee filters again, rinsed, and placed in a vial or bottle of R
828 food until eclosion. We opened a new container of hydroxyurea each month as it degrades in
829 contact with moisture and we found its potency gradually declined. We typically analyzed 5-10
830 animals (10-20 hemispheres) of each condition per batch, except in *in vivo* imaging experi-
831 ments, where we analyzed 1-5 animals per condition per batch.
832
833 Applying HU for four hours produced a somewhat U-shaped distribution, with many samples un-
834 affected and many with all four KC neuroblasts lost. Shifting from 3, to 5, to 10 mg over this long

time scale shifted how many brains were completely ablated versus unaffected, but did little to increase the proportion of brains with intermediate phenotypes. Applying the stronger concentration, 10mg, for a shorter time produced more sporadic effects, with more brains showing 1, 2, or 3 KC neuroblasts remaining. lNB/BAlc was more affected by HU concentration than time of application, with stronger effects seen applying 10mg/mL for one hour than applying 3 or 5mg/mL for four hours. Overall, combining these different protocols allowed us to observe a broad range of mushroom body states.

Immunostainings: Brains were dissected for up to 20 minutes in external saline (108 mM NaCl, 5 mM KCl, 2 mM CaCl2, 8.2 mM MgCl2, 4 mM NaHCO3, 1 mM NaH2PO4, 5 mM trehalose, 10 mM sucrose, 5 mM HEPES pH7.5, osmolarity adjusted to 265 mOsm), before being transferred to 1% paraformaldehyde in PBS, on ice. All steps were performed in cell strainer baskets (caps of FACS tubes) in 24 well plates, with the brains in the baskets lifted from well to well to change solutions. Brains were fixed overnight at 4C in 1% PFA in PBS. On day 2, brains were washed 3x10' in PBS supplemented with 0.1% triton-x-100 on a shaker at room temperature, blocked 1 hour in PBS, 0.1% triton, 4% Normal Goat Serum, and then incubated for at least two overnights in primary antibody solution, diluted in PBS, 0.1% triton, 4% Normal Goat Serum. Primary antibody was washed 3x10' in PBS supplemented with 0.1% triton-x-100 on a shaker at room temperature, then brains were incubated in secondary antibodies for at least two overnights, diluted in PBS, 0.1% triton, 4% Normal Goat Serum. When used, Alexa 568-conjugated phalloidin (1:80) and/or DAPI (1 microgram/mL) were included in secondary antibody mixes. Primary antibodies used were mouse anti-ChAT 9E10 (DSHB, 1:200), Rabbit anti-dsRed (Clontech, 1:500-1:1000), Sheep anti-GFP (Bio-Rad, 4745-1051, 1:250-1:1000), Chicken anti-GFP (1:5000, gift from Dawen Cai). Secondary antibodies were Alexa 488, 568, and 647 conjugates (1:500, Invitrogen).

Brains were mounted in 1x PBS, 90% glycerol supplemented with propyl gallate in binder reinforcement stickers sandwiched between two coverslips. Samples were stored at 4C in the dark prior to imaging. The coverslip sandwiches were taped to slides, allowing us to perform confocal imaging on one side of the brain and then flip over the sandwich to allow a clear view of the other side of the brain. This allowed us to score features on the anterior and posterior sides of each sample. Scanning confocal stacks were collected along the anterior-posterior axis on a Zeiss 880 or Leica SP8 with 1 micrometer spacing in Z and ~200nm axial resolution.

Statistical considerations: Determination of sample size: Brains were prepared for imaging in batches of 5-10. In initial batches, we assessed the variability of the manipulation, e.g. if we were trying to change Kenyon cell number, we looked at how variable the size of the Kenyon cell population was following the manipulation. We used this variability to determine how many batches to analyze so as to obtain enough informative samples. To avoid introducing statistical bias, we did not analyze the effect of the manipulation on the other cell type until after completing all batches; e.g. if the manipulation was intended to alter Kenyon cell numbers, we did not assess projection neuron bouton phenotypes until completing all samples. Genotypes or conditions being compared with one another were always prepared for staining together and imaged interspersed with one another to equalize batch effects, and we used at least two batches for each type of experiment.

Criteria for exclusion, treatment of outliers: In Figures 1-6, we only excluded from analysis samples with overt physical damage to the cells or structures being measured. In figures and analyses we treated outliers the same way as other data points. For Figure 7, full criteria for inclusion and exclusion of each sample are shown under *Analysis of KC somatic odor responses*, below.

886
887 Use of statistical tests: Recent discussions among experts have suggested that biological stud-
888 ies over-rely on statistical tests, report ρ values when statistical differences are self-evident, and
889 emphasize statistical significance rather than effect size (Goedhart, 2018a, 2018b; Ho et al.,
890 2019). These choices can cloud findings instead of clarifying them. In order to communicate our
891 findings in the simplest and most complete way, we have displayed each data point for each
892 sample to allow readers to assess effect size and significance directly.
893 *Image analysis:* In general, we analyzed mixed-sex populations, where sex ratios were carefully
894 balanced across experimental conditions. Because MZ19 labels the sexually dimorphic DA1
895 PNs, in MZ19 experiments we analyzed the two sexes independently in pilot experiments. As
896 we observed no correlation with sex (not shown), in subsequent MZ19 experiments we used
897 mixed sexes.
898
899 Researchers performing quantification could not generally be blinded to experimental condition
900 due to the overt changes in neuron numbers and brain structures induced by our manipulations.
901 However, analysis was performed blind to the goals of the experiment when possible, and quan-
902 titation of features on the anterior and posterior sides of the brain were recorded independent of
903 one another and merged after all quantifications were completed. Moreover, many of our anal-
904 yses make use of variation within an experimental condition or genotype, providing an additional
905 bulwark against observational bias.
906
907 To measure neuropil structures such as the mushroom body calyx, lateral horn, or antennal
908 lobe, we used markers such as ChAT and phalloidin to visualize the structure, identified its larg-
909 est extent in Z (i.e. along the A-P axis), outlined it in FIJI (as in white outlines in Figure F1B) and
910 then calculated the cross-sectional area using the “Measure” command.
911
912 To analyze calyx volumes we used ImageJ. Briefly, we drew Regions of Interest (ROIs) around
913 the MB247 (Figure 1) or OK107 (Figure 3) calyx signal for each slice. Other imaging channels
914 displaying projection neurons and nc82 staining were used as a reference. The drawn ROIs for
915 each slice were saved using the ROI manager plugin and the area of each ROI in a stack was
916 measured using the Measure tool. The measured areas were added together and then multi-
917 plied by the Z-spacing between slices (1 micron) to get the volume of the combined ROI through
918 the stack. The 3D viewer plugin was used to make movies of the kenyon cell and calyx vol-
919 umes. To produce 3D Movies of the calyx volumes without somata, areas outside the selected
920 ROIs were cleared and then the 3D viewer plugin was used to display only the 3D ROI volume
921 that was measured for the volume analysis. To facilitate comparison in 3D movies, stacks in a
922 set were all given the same depth in Z by adding blank slices at the end of the stack when nec-
923 essary.
924
925 To count aggregate boutons, we used ChAT signal with reference to phalloidin (which stains ac-
926 tin-rich structures, including KC dendrites), except in Figure 1 and Figure 3A, where we counted
927 GH146-positive boutons. We counted as separate structures ChAT signals that were compact
928 and appeared discontinuous with one another and that were 2+ micrometers in diameter (Figure
929 1-figure supplement 2). When phalloidin signal or KC fluorescence was available, two boutons
930 would be counted separately if ChAT signals were separated by phalloidin signal or KC signal.
931 In initial analyses, we found that boutons in slice 0 often appeared in slices -1 and +1 as well,
932 but never in slices -2 or +2. In order to avoid counting the same boutons more than once, we
933 therefore began counting at the most anterior slice in the stack where boutons were visible, and
934 counted every other slice, i.e. every second micron. To count boutons of small groups of PNs,
935 we drove fluorescent reporters under control of 42D01, 71D09, or MZ19 and counted coherent
936 and compact fluorescent signals, with reference to ChAT signals and to phalloidin, when

available. As GH146 labels ~2/3 of PNs, our counts of 450-650 total GH146+ boutons in Figures 1 and 3, which would correspond to 675-975 total boutons per calyx, correspond with estimates established by EM (578 boutons) and light microscopy (768 total boutons, 5 boutons per PN) (Leiss et al., 2009; Turner et al., 2008; Zheng et al., 2018).

To count cell populations, we used genetically-encoded fluorescence as indicated. We counted labeled somata in every third slice in the stack (every third micron along the A-P axis), with reference to DAPI to distinguish individual cells from one another. As we did for boutons, in analyzing somata we initially determined that somata in slice 0 could also be seen in slices -2, -1, +1, and +2 but not in slice -3 or +3. To avoid double-counting, we therefore counted every third micron.

To count KC claws, we scanned image stacks for cup-shaped terminal structures of the appropriate size (1-2μm in diameter). We sometimes labeled small groups of KCs. We scored independently any single KC or small group of KCs that could be visually separated from one another (like the 3 cells shown in Figure 6C). For Figure 2 and Figure 2-figure supplement 3, we did not score any cells which we could not separate from one another because we did not want to mix counts for KCs of different types. For Figure 3I, where we did not attempt to separate KCs of different types, and Figure 6F, where our dye labeling strategy was specific to αβ KCs, we present an average claw/KC data point for small groups of 2-4 cells whose dendritic structures were interwoven. Finally, in Figure 3I, we found that in calyces with expanded KC populations, KC axons sometimes could not enter the pedunculus and instead wandered around at the base of the calyx. As CNS neurons in *D. mel* are unipolar, these wandering axons could be difficult to distinguish from dendritic claws. To determine whether these wandering axons should be counted as claws, we stained a subset of photoactivated brains with anti-ChAT (not shown), to determine which labeled KC neurites were in the bouton region of the calyx, and should thus be scored for claws, and which were “lost” axons. Though photoactivated GFP signals were only poorly preserved following staining, relating ChAT-stained images to images of the same brain by two photon allowed us to learn to identify the bouton region of the calyx in subsequent experiments due to its “swiss cheese” appearance, where the presence of PN boutons produces holes in KC fluorescence.

To determine KC and PN neuroblast state--PN lNB/BAlc: Whenever possible, we included GH146 or 60A10 driving a fluorescent report in our animals and scored the presence or absence of a group of somata lateral to the antennal lobe on the anterior side of the brain for each analyzed hemisphere. KC neuroblasts: In Figures 2A-C, we used 58F02 to fluorescently label late-born KCs and counted clumps of labeled somata surrounding the calyx as well as groups of labeled neurites leaving the calyx and entering the pedunculus. These estimates usually matched; in the few cases where they did not, we used the number of axon clumps, as somata are closer to the surface of the brain and more susceptible to mechanical disruption during dissection. As seen in Figure 2B, 58F02 labels additional neurons; these were easy to discriminate from KCs as they did not enter the calyx or pedunculus.

For Figures 2J, K and Figure 2-figure supplement 3C, D, we combined data from two different types of experiments. In some experiments, we expressed PA-GFP in all KCs using MB247. We traced the axons of labeled KCs into the lobes to assign KC type (Figure 2-figure supplement 3). In a second group of experiments, we used 58F02-Gal4 to express PA-GFP exclusively in αβ core KCs (Figure 2I), or 89B01 Gal4 to express PA-GFP only in γ KCs and thus knew KC type a priori. 89B01 also labels γ d KCs, which can be distinguished from olfactory γ KCs as they do not innervate the main calyx. We do not include γd KCs in our analysis,

GFP photoactivation and Texas red dextran dye labeling were performed as previously described (Clowney et al., 2015; Ruta et al., 2010), using a Bruker Investigator microscope and Spectra-Physics MaiTai laser with DeepSee module. Dye filling electrodes were pulled using a Brown/Flaming puller (Sutter Instruments) and were guided to the mushroom body alpha lobes using visible light illumination and/or two photon autofluorescence.

Identification of driver lines for relevant cell populations: To identify Gal4 and/or LexA lines labeling PN populations, we screened the Janelia FlyLight collection online database and then crossed lines with potential to fluorescent reporters. While 42D01 (~10PNs) and 60A10 (60 PNs) were the most useful PN lines for us here, we also identified other lines, 33C10 and 37H08, that each label small groups of PNs and may be of use to others. To identify Gal4 lines labeling individual KC types, we screened expression of "regular" FlyLight Gal4 constructs made using the same regulatory fragments incorporated in KC-type-specific split Gal4s (Aso et al., 2014). We found 58F02 useful for labeling α/β core KCs, 89B01 for γ KCs (labels both γmain and γd), and 41C07 for α'/β' KCs. 89B01 and 58F02 LexA did not recapitulate Gal4 expression patterns driven by the same fragments.

Flow Cytometry: Brains were dissected in Schneider's medium (Sigma S0146) supplemented with 1% BSA and placed on ice. After all dissections were completed, collagenase (Sigma C0130) was added to a final concentration of 2mg/mL and samples were incubated at 37C for 20 minutes. Samples were dissociated by trituration and spun down at 300g, 4C, for 5 minutes. Collagenase solution was removed and replaced with PBS+0.1% BSA supplemented with 1:1000 DyeCycle Violet. Cells were incubated with dye for 30 minutes on ice and passed through a cell strainer cap, before being subjected to flow cytometry on an Attune Flow Cytometer. Forward scatter and side scatter measurements were used to gate single cells, and DyeCycle Violet signal was used to gate cell bodies from membrane debris.

In vivo functional imaging: We prepared 2-7 day old adult flies subjected to HU or sham treatment just after larval hatching for *in vivo* two photon calcium imaging on a Bruker Investigator essentially as described previously (Ruta et al., 2010), affixing the fly to packaging tape (Duck EZ Start) with human hair and UV glue (Loctite 3106). The fly was tilted to allow optical access to KC somata, at the dorsal posterior surface of the brain. In some experiments, we waxed the proboscis in an extended position to reduce motion. Imaging was performed in external saline. For odor delivery, half of a 1200mL/min airstream, or 600mL/min, was directed toward the antennae through a Pasteur pipette mounted on a micromanipulator. At a trigger, 25% of the total air stream was re-directed from a 10mL glass vial containing mineral oil to a vial containing odorants diluted 1:10 in mineral oil. Final odor dilution was therefore 1:40. Filter paper "wicks" were inserted into each vial to allow odor to saturate the vial headspace. Odors were delivered for two seconds, with 30-60 seconds in between stimulations. We used a simplified olfactometer capable of delivering five different odorants in which overall airflow was metered by analogue flowmeters (Brooks Instruments) and valve switching controlled by an Arduino. Odor delivery was initially optimized using a mini-PID placed in the half of the air stream not directed at the fly (Aurora Biosciences). Images were collected at 1.5-5 Hertz, and we imaged a single plane for each sample.

Analysis of KC somatic odor responses: We collected data from a total of 14 sham-treated animals (28 hemispheres imaged) and 24 HU-treated animals (46 hemispheres imaged). The two hemispheres were imaged separately. Occasionally, only one hemisphere was imaged due to the preparation and a few hemispheres were excluded from analysis because of poor image quality. Mineral oil was delivered first, and then each of four odors was delivered twice, in

sequence. Following mineral oil, odor order varied. Because experiments in locust found that the first presentation of certain odors can cause distinct KC responses to all subsequent presentations of that same odor, we analyzed the second presentation of each odor, according to convention (Murthy et al., 2008; Stopfer and Laurent, 1999). We also observed that in some animals, enduring increases in fluorescence followed the first presentation of isobutyl acetate.

Following functional imaging, we either collected a Z-stack of the mushroom body on the two-photon, or dissected out the brain and subjected it to immunostatining and confocal imaging. We used these images to categorize the extent of KC reduction. All samples are accounted for here:

	Total hem	Poor image	Damaged/ not respon-sive	un-known	Full ablation	can't tell if ablated	Doesn't look ablated	Too much motion	analyzed
Sham	28	2	8	1	N/A	N/A	N/A	10	7: 4 fem, 3 male
HU	46		4	0	13	5	10	7	7: 4 male, 3 fem

We excluded 11 hemispheres from the control dataset due to damage or poor image quality. We also excluded 34 hemispheres from the ablation dataset because of any of the following: the samples were fully ablated, unaffected by ablation, ablation status was ambiguous, or the mushroom body calyx appeared damaged. The remaining samples were motion-corrected using Suite2p (Pachitariu et al., 2017). Using FIJI, we blinded ourselves to the remaining datasets and excluded datasets if there was too much motion to be able to follow the same cell over time. After this gate, there were 7 sham and 7 reduced-KC hemispheres for the analysis. ROIs were chosen in each of the fourteen samples and we measured Df/f (i.e. (f-f0)/f0), comparing stimulus frames with pre-stimulus frames. ROIs were manually chosen and we were careful about ensuring that the cell remained within its ROI for all frames. For two of the ablated samples, we had to choose different ROIs for two of the odor deliveries due to motion. These samples were only used to calculate the proportion of cells that were responsive to each odor, and not in calculating the number of odors each cell responded to. The baseline was determined for each odor delivery by taking the average of the frames that were three seconds before the trigger. The stimulus frame was determined by taking the peak response between 0–4.5 s after stimulus onset, to account for the valve opening and the two second odor delivery. To define "responsive" cells, we chose to use the same cutoff, Df/f >0.2 (20% increase in fluorescence over baseline) across samples. This was in order to avoid obscuring overall differences in responsiveness across ablated and sham-treated calyces. For visualization, we used the Pretty Heatmap package in R to cluster cells with similar odor responses and display them.

References

Akerboom J, Chen T-W, Wardill TJ, Tian L, Marvin JS, Mutlu S, Calderón NC, Esposti F, Borghuis BG, Sun XR, Gordus A, Orger MB, Portugues R, Engert F, Macklin JJ, Filosa A, Aggarwal A, Kerr RA, Takagi R, Kracun S, Shigetomi E, Khakh BS, Baier H, Lagnado L, Wang SS-H, Bargmann CI, Kimmel BE, Jayaraman V, Svoboda K, Kim DS, Schreiter ER, Looger LL. 2012. Optimization of a GCaMP calcium indicator for neural activity imaging. *J Neurosci Off J Soc Neurosci* **32**:13819–13840. doi:10.1523/JNEUROSCI.2601-12.2012

Albus JS. 1971. A theory of cerebellar function. *Math Biosci* **10**:25–61. doi:10.1016/0025-5564(71)90051-4

Aso Y, Hattori D, Yu Y, Johnston RM, Iyer NA, Ngo T-TB, Dionne H, Abbott LF, Axel R, Tanimoto H, Rubin GM. 2014. The neuronal architecture of the mushroom body provides a logic for associative learning. *eLife* **3**:e04577. doi:10.7554/eLife.04577

Awasaki T, Kao C-F, Lee Y-J, Yang C-P, Huang Y, Pfeiffer BD, Luan H, Jing X, Huang Y-F, He Y, Schroeder MD, Kuzin A, Brody T, Zugates CT, Odenwald WF, Lee T. 2014. Making *Drosophila* lineage–restricted drivers via patterned recombination in neuroblasts. *Nat Neurosci* **17**:631. doi:10.1038/nn.3654

Bell CC, Han V, Sawtell NB. 2008. Cerebellum-like structures and their implications for cerebellar function. *Annu Rev Neurosci* **31**:1–24. doi:10.1146/annurev.neuro.30.051606.094225

Berdnik D, Chihara T, Couto A, Luo L. 2006. Wiring Stability of the Adult Drosophila Olfactory Circuit after Lesion. *J Neurosci* **26**:3367–3376. doi:10.1523/JNEUROSCI.4941-05.2006

Caron SJC, Ruta V, Abbott LF, Axel R. 2013. Random convergence of olfactory inputs in the Drosophila mushroom body. *Nature* **497**:113–117. doi:10.1038/nature12063

Cayco-Gajic NA, Clopath C, Silver RA. 2017. Sparse synaptic connectivity is required for decorrelation and pattern separation in feedforward networks. *Nat Commun* **8**:1116. doi:10.1038/s41467-017-01109-y

Chen Y, Akin O, Nern A, Tsui CYK, Pecot MY, Zipursky SL. 2014. Cell-type-Specific Labeling of Synapses In Vivo through Synaptic Tagging with Recombination. *Neuron* **81**:280–293. doi:10.1016/j.neuron.2013.12.021

Chin SG, Maguire SE, Huoviala P, Jefferis GSXE, Potter CJ. 2018. Olfactory Neurons and Brain Centers Directing Oviposition Decisions in Drosophila. *Cell Rep* **24**:1667–1678. doi:10.1016/j.celrep.2018.07.018

Clowney EJ, Iguchi S, Bussell JJ, Scheer E, Ruta V. 2015. Multimodal Chemosensory Circuits Controlling Male Courtship in Drosophila. *Neuron* **87**:1036–1049. doi:10.1016/j.neuron.2015.07.025

Cohn R, Morantte I, Ruta V. 2015. Coordinated and Compartmentalized Neuromodulation Shapes Sensory Processing in Drosophila. *Cell* **163**:1742–1755. doi:10.1016/j.cell.2015.11.019

Connolly JB, Roberts IJH, Armstrong JD, Kaiser K, Forte M, Tully T, O'Kane CJ. 1996. Associative Learning Disrupted by Impaired Gs Signaling in Drosophila Mushroom Bodies. *Science* **274**:2104–2107. doi:10.1126/science.274.5295.2104

Corty MM, Tam J, Grueber WB. 2016. Dendritic diversification through transcription factor-mediated suppression of alternative morphologies. *Development* **143**:1351–1362. doi:10.1242/dev.130906

Das A, Gupta T, Davla S, Prieto-Godino LL, Diegelmann S, Reddy OV, Raghavan KV, Reichert H, Lovick J, Hartenstein V. 2013. Neuroblast lineage-specific origin of the neurons of the

Drosophila larval olfactory system. *Dev Biol* **373**:322–337. doi:10.1016/j.ydbio.2012.11.003

de Belle JS, Heisenberg M. 1994. Associative odor learning in Drosophila abolished by chemical ablation of mushroom bodies. *Science* **263**:692–695.

Eichler K, Li F, Litwin-Kumar A, Park Y, Andrade I, Schneider-Mizell CM, Saumweber T, Huser A, Eschbach C, Gerber B, Fetter RD, Truman JW, Priebe CE, Abbott LF, Thum AS, Zlatic M, Cardona A. 2017. The complete connectome of a learning and memory centre in an insect brain. *Nature* **548**:175–182. doi:10.1038/nature23455

Fan H, Favero M, Vogel MW. 2001. Elimination of bax expression in mice increases cerebellar purkinje cell numbers but not the number of granule cells. *J Comp Neurol* **436**:82–91. doi:10.1002/cne.1055

Farris SM. 2011. Are mushroom bodies cerebellum-like structures? *Arthropod Struct Dev* **40**:368–379. doi:10.1016/j.asd.2011.02.004

Fişek M, Wilson RI. 2014. Stereotyped connectivity and computations in higher-order olfactory neurons. *Nat Neurosci* **17**:280–288. doi:10.1038/nn.3613

Frank DD, Jouandet GC, Kearney PJ, Macpherson LJ, Gallio M. 2015. Temperature representation in the Drosophila brain. *Nature* **519**:358–361. doi:10.1038/nature14284

Gibbins IL, Teo EH, Jobling P, Morris JL. 2003. Synaptic density, convergence, and dendritic complexity of prevertebral sympathetic neurons. *J Comp Neurol* **455**:285–298. doi:10.1002/cne.10404

Goedhart J. 2018a. Dispense with redundant P values. *Nature* **554**:31–31. doi:10.1038/d41586-018-01314-9

Goedhart J. 2018b. Prevent p-value parroting. *the Node*. https://thenode.biologists.com/p-value-parroting/research/

Grabe V, Baschwitz A, Dweck HKM, Lavista-Llanos S, Hansson BS, Sachse S. 2016. Elucidating the Neuronal Architecture of Olfactory Glomeruli in the Drosophila Antennal Lobe. *Cell Rep* **16**:3401–3413. doi:10.1016/j.celrep.2016.08.063

Gruntman E, Turner GC. 2013. Integration of the olfactory code across dendritic claws of single mushroom body neurons. *Nat Neurosci* **16**:1821–1829. doi:10.1038/nn.3547

Guan Z, Prado A, Melzig J, Heisenberg M, Nash HA, Raabe T. 2000. Mushroom body defect, a gene involved in the control of neuroblast proliferation in Drosophila, encodes a coiled–coil protein. *Proc Natl Acad Sci* **97**:8122–8127. doi:10.1073/pnas.97.14.8122

Han DD, Stein D, Stevens LM. 2000. Investigating the function of follicular subpopulations during Drosophila oogenesis through hormone-dependent enhancer-targeted cell ablation. *Dev Camb Engl* **127**:573–583.

Handler A, Graham TGW, Cohn R, Morantte I, Siliciano AF, Zeng J, Li Y, Ruta V. 2019. Distinct Dopamine Receptor Pathways Underlie the Temporal Sensitivity of Associative Learning. *Cell* **178**:60-75.e19. doi:10.1016/j.cell.2019.05.040

Hige T. 2018. What can tiny mushrooms in fruit flies tell us about learning and memory? *Neurosci Res* **129**:8–16. doi:10.1016/j.neures.2017.05.002

Hige T, Aso Y, Rubin GM, Turner GC. 2015. Plasticity-driven individualization of olfactory coding in mushroom body output neurons. *Nature* **526**:258–262. doi:10.1038/nature15396

Ho J, Tumkaya T, Aryal S, Choi H, Claridge-Chang A. 2019. Moving beyond P values: data analysis with estimation graphics. *Nat Methods* **16**:565–566. doi:10.1038/s41592-019-0470-3

1165 Honegger KS, Campbell RAA, Turner GC. 2011. Cellular-resolution population imaging reveals
1166 robust sparse coding in the Drosophila mushroom body. *J Neurosci Off J Soc Neurosci*
1167 **31**:11772–11785. doi:10.1523/JNEUROSCI.1099-11.2011
1168 Hong W, Mosca TJ, Luo L. 2012. Teneurins instruct synaptic partner matching in an olfactory
1169 map. *Nature* **484**:201–207. doi:10.1038/nature10926
1170 Hume RI, Purves D. 1983. Apportionment of the terminals from single preganglionic axons to
1171 target neurones in the rabbit ciliary ganglion. *J Physiol* **338**:259–275. doi:10.1113/jphys-
1172 iol.1983.sp014672
1173 Hume RI, Purves D. 1981. Geometry of neonatal neurones and the regulation of synapse elimi-
1174 nation. *Nature* **293**:469–471.
1175 Ito K, Awano W, Suzuki K, Hiromi Y, Yamamoto D. 1997. The Drosophila mushroom body is a
1176 quadruple structure of clonal units each of which contains a virtually identical set of neu-
1177 rones and glial cells. *Development* **124**:761–771.
1178 Ito K, Hotta Y. 1992. Proliferation pattern of postembryonic neuroblasts in the brain of Drosoph-
1179 ila melanogaster. *Dev Biol* **149**:134–148. doi:10.1016/0012-1606(92)90270-Q
1180 Jan Y-N, Jan LY. 2010. Branching out: mechanisms of dendritic arborization. *Nat Rev Neurosci*
1181 **11**:316–328. doi:10.1038/nrn2836
1182 Jefferis GSXE, Potter CJ, Chan AM, Marin EC, Rohlfing T, Maurer CR, Luo L. 2007. Compre-
1183 hensive maps of Drosophila higher olfactory centers: spatially segregated fruit and phero-
1184 mone representation. *Cell* **128**:1187–1203. doi:10.1016/j.cell.2007.01.040
1185 Jefferis GSXE, Vyas RM, Berdnik D, Ramaekers A, Stocker RF, Tanaka NK, Ito K, Luo L.
1186 2004. Developmental origin of wiring specificity in the olfactory system of Drosophila.
1187 *Dev Camb Engl* **131**:117–130. doi:10.1242/dev.00896
1188 Jenett A, Rubin GM, Ngo T-TB, Shepherd D, Murphy C, Dionne H, Pfeiffer BD, Cavallaro A,
1189 Hall D, Jeter J, Iyer N, Fetter D, Hausenfluck JH, Peng H, Trautman ET, Svirskas RR,
1190 Myers EW, Iwinski ZR, Aso Y, DePasquale GM, Enos A, Hulamm P, Lam SCB, Li H-H,
1191 Laverty TR, Long F, Qu L, Murphy SD, Rokicki K, Safford T, Shaw K, Simpson JH,
1192 Sowell A, Tae S, Yu Y, Zugates CT. 2012. A GAL4-Driver Line Resource for Drosoph-
1193 ila Neurobiology. *Cell Rep* **2**:991–1001. doi:10.1016/j.celrep.2012.09.011
1194 Keene AC, Waddell S. 2007. Drosophila olfactory memory: single genes to complex neural cir-
1195 cuits. *Nat Rev Neurosci* **8**:341–354. doi:10.1038/nrn2098
1196 Kennedy A. 2019. Learning with naturalistic odor representations in a dynamic model of the
1197 Drosophila olfactory system | bioRxiv. *bioRxiv*. doi:https://doi.org/10.1101/783191
1198 Kennedy A. 2015. Representation and learning in cerebellum-like structures. Columbia Univer-
1199 sity. doi:10.7916/D8DV1HM1
1200 Kirkhart C, Scott K. 2015. Gustatory Learning and Processing in the Drosophila Mushroom Bod-
1201 ies. *J Neurosci* **35**:5950–5958. doi:10.1523/JNEUROSCI.3930-14.2015
1202 Kohara K, Kitamura A, Adachi N, Nishida M, Itami C, Nakamura S, Tsumoto T. 2003. Inhibi-
1203 tory But Not Excitatory Cortical Neurons Require Presynaptic Brain-Derived Neu-
1204 rotrophic Factor for Dendritic Development, as Revealed by Chimera Cell Culture. *J*
1205 *Neurosci* **23**:6123–6131. doi:10.1523/JNEUROSCI.23-14-06123.2003
1206 Kvon EZ, Kazmar T, Stampfel G, Yáñez-Cuna JO, Pagani M, Schernhuber K, Dickson BJ, Stark
1207 A. 2014. Genome-scale functional characterization of Drosophila developmental enhanc-
1208 ers in vivo. *Nature* **512**:91–95. doi:10.1038/nature13395

1209 Lai S-L, Awasaki T, Ito K, Lee T. 2008. Clonal analysis of Drosophila antennal lobe neurons:
1210 diverse neuronal architectures in the lateral neuroblast lineage. *Dev Camb Engl*
1211 **135**:2883–2893. doi:10.1242/dev.024380
1212 Lai S-L, Lee T. 2006. Genetic mosaic with dual binary transcriptional systems in Drosophila.
1213 *Nat Neurosci* **9**:703–709. doi:10.1038/nn1681
1214 Lee T, Lee A, Luo L. 1999. Development of the Drosophila mushroom bodies: sequential gener-
1215 ation of three distinct types of neurons from a neuroblast. *Development* **126**:4065–4076.
1216 Lee T, Luo L. 1999. Mosaic analysis with a repressible cell marker for studies of gene function
1217 in neuronal morphogenesis. *Neuron* **22**:451–461.
1218 Leiss F, Groh C, Butcher NJ, Meinertzhagen IA, Tavosanis G. 2009. Synaptic organization in the
1219 adult Drosophila mushroom body calyx. *J Comp Neurol* **517**:808–824.
1220 doi:10.1002/cne.22184
1221 Lin AC, Bygrave AM, de Calignon A, Lee T, Miesenböck G. 2014. Sparse, decorrelated odor
1222 coding in the mushroom body enhances learned odor discrimination. *Nat Neurosci*
1223 **17**:559–568. doi:10.1038/nn.3660
1224 Litwin-Kumar A, Harris KD, Axel R, Sompolinsky H, Abbott LF. 2017. Optimal Degrees of
1225 Synaptic Connectivity. *Neuron* **93**:1153-1164.e7. doi:10.1016/j.neuron.2017.01.030
1226 Liu Z, Yang C-P, Sugino K, Fu C-C, Liu L-Y, Yao X, Lee LP, Lee T. 2015. Opposing intrinsic
1227 temporal gradients guide neural stem cell production of varied neuronal fates. *Science*
1228 **350**:317–320. doi:10.1126/science.aad1886
1229 Lovick JK, Hartenstein V. 2015. Hydroxyurea-mediated neuroblast ablation establishes birth
1230 dates of secondary lineages and addresses neuronal interactions in the developing Dro-
1231 sophila brain. *Dev Biol* **402**:32–47. doi:10.1016/j.ydbio.2015.03.005
1232 Lovick JK, Kong A, Omoto JJ, Ngo KT, Younossi-Hartenstein A, Hartenstein V. 2016. Patterns
1233 of growth and tract formation during the early development of secondary lineages in the
1234 Drosophila larval brain. *Dev Neurobiol* **76**:434–451. doi:10.1002/dneu.22325
1235 Marin EC, Watts RJ, Tanaka NK, Ito K, Luo L. 2005. Developmentally programmed remodeling
1236 of the Drosophila olfactory circuit. *Dev Camb Engl* **132**:725–737. doi:10.1242/dev.01614
1237 Marr D. 1969. A theory of cerebellar cortex. *J Physiol* **202**:437–470. doi:10.1113/jphys-
1238 iol.1969.sp008820
1239 Masuda-Nakagawa LM, Tanaka NK, O'Kane CJ. 2005. Stereotypic and random patterns of con-
1240 nectivity in the larval mushroom body calyx of Drosophila. *Proc Natl Acad Sci*
1241 **102**:19027–19032. doi:10.1073/pnas.0509643102
1242 McAllister AK, Katz LC, Lo DC. 1997. Opposing roles for endogenous BDNF and NT-3 in reg-
1243 ulating cortical dendritic growth. *Neuron* **18**:767–778.
1244 McAllister AK, Lo DC, Katz LC. 1995. Neurotrophins regulate dendritic growth in developing
1245 visual cortex. *Neuron* **15**:791–803. doi:10.1016/0896-6273(95)90171-X
1246 Meng JL, Marshall ZD, Lobb-Rabe M, Heckscher ES. 2019. How prolonged expression of
1247 Hunchback, a temporal transcription factor, re-wires locomotor circuits. *eLife* **8**:e46089.
1248 doi:10.7554/eLife.46089
1249 Mugnaini E, Osen KK, Dahl AL, Friedrich VL, Korte G. 1980. Fine structure of granule cells
1250 and related interneurons (termed Golgi cells) in the cochlear nuclear complex of cat, rat
1251 and mouse. *J Neurocytol* **9**:537–570.
1252 Murthy M, Fiete I, Laurent G. 2008. Testing Odor Response Stereotypy in the Drosophila Mush-
1253 room Body. *Neuron* **59**:1009–1023. doi:10.1016/j.neuron.2008.07.040

Muthukumar AK, Stork T, Freeman MR. 2014. Activity-dependent regulation of astrocyte GAT levels during synaptogenesis. *Nat Neurosci* **17**:1340–1350. doi:10.1038/nn.3791

Owald D, Waddell S. 2015. Olfactory learning skews mushroom body output pathways to steer behavioral choice in Drosophila. *Curr Opin Neurobiol* **35**:178–184. doi:10.1016/j.conb.2015.10.002

Pachitariu M, Stringer C, Dipoppa M, Schröder S, Rossi LF, Dalgleish H, Carandini M, Harris KD. 2017. Suite2p: beyond 10,000 neurons with standard two-photon microscopy. *bioRxiv* 061507. doi:10.1101/061507

Pauls D, Selcho M, Gendre N, Stocker RF, Thum AS. 2010. Drosophila larvae establish appetitive olfactory memories via mushroom body neurons of embryonic origin. *J Neurosci Off J Soc Neurosci* **30**:10655–10666. doi:10.1523/JNEUROSCI.1281-10.2010

Perkins LA, Holderbaum L, Tao R, Hu Y, Sopko R, McCall K, Yang-Zhou D, Flockhart I, Binari R, Shim H-S, Miller A, Housden A, Foos M, Randkelv S, Kelley C, Namgyal P, Villalta C, Liu L-P, Jiang X, Huan-Huan Q, Wang X, Fujiyama A, Toyoda A, Ayers K, Blum A, Czech B, Neumuller R, Yan D, Cavallaro A, Hibbard K, Hall D, Cooley L, Hannon GJ, Lehmann R, Parks A, Mohr SE, Ueda R, Kondo S, Ni J-Q, Perrimon N. 2015. The Transgenic RNAi Project at Harvard Medical School: Resources and Validation. *Genetics* **201**:843–852. doi:10.1534/genetics.115.180208

Pfeiffer BD, Truman JW, Rubin GM. 2012. Using translational enhancers to increase transgene expression in Drosophila. *Proc Natl Acad Sci U S A* **109**:6626–6631. doi:10.1073/pnas.1204520109

Pitman JL, Huetteroth W, Burke CJ, Krashes MJ, Lai S-L, Lee T, Waddell S. 2011. A Pair of Inhibitory Neurons Are Required to Sustain Labile Memory in the Drosophila Mushroom Body. *Curr Biol* **21**:855–861. doi:10.1016/j.cub.2011.03.069

Pop S, Chen C-L, Sproston CJ, Kondo S, Ramdya P, Williams DW. 2019. Patterned cell death sculpts functional and adaptive neural networks in flies. *bioRxiv* 626465. doi:10.1101/626465

Potter CJ, Tasic B, Russler EV, Liang L, Luo L. 2010. The Q System: A Repressible Binary System for Transgene Expression, Lineage Tracing and Mosaic Analysis. *Cell* **141**:536–548. doi:10.1016/j.cell.2010.02.025

Prieto-Godino LL, Silbering AF, Khallaf MA, Cruchet S, Bojkowska K, Pradervand S, Hansson BS, Knaden M, Benton R. 2019. Functional integration of "undead" neurons in the olfactory system. *bioRxiv* 623488. doi:10.1101/623488

Prokop A, Technau GM. 1994. Normal Function of the mushroom body defect Gene of Drosophila Is Required for the Regulation of the Number and Proliferation of Neuroblasts. *Dev Biol* **161**:321–337. doi:10.1006/dbio.1994.1034

Purves D. 1986. The trophic theory of neural concentrations. *Trends Neurosci* **9**:486–489. doi:10.1016/0166-2236(86)90155-4

Purves D, Hume RI. 1981. The relation of postsynaptic geometry to the number of presynaptic axons that innervate autonomic ganglion cells. *J Neurosci Off J Soc Neurosci* **1**:441–452.

Ramaekers A, Magnenat E, Marin EC, Gendre N, Jefferis GSXE, Luo L, Stocker RF. 2005. Glomerular maps without cellular redundancy at successive levels of the Drosophila larval olfactory circuit. *Curr Biol CB* **15**:982–992. doi:10.1016/j.cub.2005.04.032

Riemensperger T, Völler T, Stock P, Buchner E, Fiala A. 2005. Punishment prediction by dopaminergic neurons in Drosophila. *Curr Biol CB* **15**:1953–1960. doi:10.1016/j.cub.2005.09.042

1300 Ruta V, Datta SR, Vasconcelos ML, Freeland J, Looger LL, Axel R. 2010. A dimorphic phero-
1301 mone circuit in Drosophila from sensory input to descending output. *Nature* **468**:686–
1302 690. doi:10.1038/nature09554
1303 Seroka AQ, Doe CQ. 2019. The Hunchback temporal transcription factor determines motor neu-
1304 ron axon and dendrite targeting in Drosophila. *Development* **146**.
1305 doi:10.1242/dev.175570
1306 Shaw RE, Kottler B, Ludlow ZN, Buhl E, Kim D, Silva SM da, Miedzik A, Coum A, Hodge JJ,
1307 Hirth F, Sousa-Nunes R. 2018. In vivo expansion of functionally integrated GABAergic
1308 interneurons by targeted increase in neural progenitors. *EMBO J* e98163.
1309 doi:10.15252/embj.201798163
1310 Siller KH, Cabernard C, Doe CQ. 2006. The NuMA-related Mud protein binds Pins and regu-
1311 lates spindle orientation in Drosophila neuroblasts. *Nat Cell Biol* **8**:594–600.
1312 doi:10.1038/ncb1412
1313 Stocker RF, Heimbeck G, Gendre N, de Belle JS. 1997. Neuroblast ablation in Drosophila
1314 P[GAL4] lines reveals origins of olfactory interneurons. *J Neurobiol* **32**:443–456.
1315 Stopfer M, Laurent G. 1999. Short-term memory in olfactory network dynamics. *Nature*
1316 **402**:664–668. doi:10.1038/45244
1317 Strausfeld NJ, Sinakevitch I, Brown SM, Farris SM. 2009. Ground plan of the insect mushroom
1318 body: functional and evolutionary implications. *J Comp Neurol* **513**:265–291.
1319 doi:10.1002/cne.21948
1320 Sweeney ST, Hidalgo A, Belle JS de, Keshishian H. 2012. Hydroxyurea Ablation of Mushroom
1321 Bodies in Drosophila. *Cold Spring Harb Protoc* **2012**:pdb.prot067777.
1322 doi:10.1101/pdb.prot067777
1323 Tenedini FM, González MS, Hu C, Pedersen LH, Petruzzi MM, Spitzweck B, Wang D, Richter
1324 M, Petersen M, Szpotowicz E, Schweizer M, Sigrist SJ, Anda FC de, Soba P. 2019.
1325 Maintenance of cell type-specific connectivity and circuit function requires Tao kinase.
1326 *Nat Commun* **10**:1–16. doi:10.1038/s41467-019-11408-1
1327 Turner GC, Bazhenov M, Laurent G. 2008. Olfactory representations by Drosophila mushroom
1328 body neurons. *J Neurophysiol* **99**:734–746. doi:10.1152/jn.01283.2007
1329 Turney SG, Lichtman JW. 2012. Reversing the outcome of synapse elimination at developing
1330 neuromuscular junctions in vivo: evidence for synaptic competition and its mechanism.
1331 *PLoS Biol* **10**:e1001352. doi:10.1371/journal.pbio.1001352
1332 Vogt K, Aso Y, Hige T, Knapek S, Ichinose T, Friedrich AB, Turner GC, Rubin GM, Tanimoto
1333 H. 2016. Direct neural pathways convey distinct visual information to Drosophila mush-
1334 room bodies. *eLife* **5**. doi:10.7554/eLife.14009
1335 Wang Y, Guo H-F, Pologruto TA, Hannan F, Hakker I, Svoboda K, Zhong Y. 2004. Stereotyped
1336 odor-evoked activity in the mushroom body of Drosophila revealed by green fluorescent
1337 protein-based Ca2+ imaging. *J Neurosci Off J Soc Neurosci* **24**:6507–6514.
1338 doi:10.1523/JNEUROSCI.3727-03.2004
1339 Ward A, Hong W, Favaloro V, Luo L. 2015. Toll receptors instruct axon and dendrite targeting
1340 and participate in synaptic partner matching in a Drosophila olfactory circuit. *Neuron*
1341 **85**:1013–1028. doi:10.1016/j.neuron.2015.02.003
1342 Yagi R, Mabuchi Y, Mizunami M, Tanaka NK. 2016. Convergence of multimodal sensory path-
1343 ways to the mushroom body calyx in *Drosophila melanogaster*. *Sci Rep* **6**:29481.
1344 doi:10.1038/srep29481

1345 Yu H-H, Kao C-F, He Y, Ding P, Kao J-C, Lee T. 2010. A complete developmental sequence of
1346 a Drosophila neuronal lineage as revealed by twin-spot MARCM. *PLoS Biol* **8**.
1347 doi:10.1371/journal.pbio.1000461
1348 Zheng Z, Lauritzen JS, Perlman E, Robinson CG, Nichols M, Milkie D, Torrens O, Price J,
1349 Fisher CB, Sharifi N, Calle-Schuler SA, Kmecova L, Ali IJ, Karsh B, Trautman ET, Bo-
1350 govic JA, Hanslovsky P, Jefferis GSXE, Kazhdan M, Khairy K, Saalfeld S, Fetter RD,
1351 Bock DD. 2018. A Complete Electron Microscopy Volume of the Brain of Adult Dro-
1352 sophila melanogaster. *Cell* **174**:730-743.e22. doi:10.1016/j.cell.2018.06.019
1353 Ziegler AB, Thiele C, Tenedini F, Richard M, Leyendecker P, Hoermann A, Soba P, Tavosanis
1354 G. 2017. Cell-Autonomous Control of Neuronal Dendrite Expansion via the Fatty Acid
1355 Synthesis Regulator SREBP. *Cell Rep* **21**:3346–3353. doi:10.1016/j.celrep.2017.11.069
1356
1357

1358 Legends for videos:
1359 **Figure 1-video 1:** Volume renderings of mushroom bodies shown in Figure 1B, using the Ken-
1360 yon cell (GFP) signal. The video cycles through calyces in the order shown in the Figure (1305
1361 KCs, 964 KCs, 679 KCs, 279 KCs, 97 KCs), showing first the full GFP signal (somata, calyx,
1362 lobes), and then the isolated calyx of that sample. Red bounding boxes contain the same vol-
1363 ume throughout, though the rendering program re-scales certain samples to fill the frame.
1364
1365 **Figure 3-video 1:** Volume renderings of mushroom bodies shown in Figure 3A, using the Ken-
1366 yon cell (GFP) signal. The video shows the mud-RNAi mushroom body first (3951 KCs), and
1367 then the control mushroom body (1227 KCs). For each sample, the full mushroom body is
1368 shown first, and then the isolated calyx. Red bounding boxes contain the same volume through-
1369 out.
1370
1371 **Figure 7-video 1, 2:** Full, motion-corrected functional imaging time series for one sham-treated
1372 (video 1) and one HU-treated, reduced-KC calyx (video 2). Data was collected at 5 Hz, and
1373 each series extends over the five minute presentation of four odors and mineral oil control.
1374 These are different samples than the ones shown in Figure 7A-C and Figure 7-figure supple-
1375 ment 1. The intermittently very bright cell in video 2 does not show any correlation with odor
1376 presentation and may be damaged.
1377